PSFC/JA-11-20

Scaling of H-mode threshold power and L-H edge conditions with favorable ion grad-B drift in Alcator C-Mod tokamak

Y.Ma, J.W.Hughes, A.E.Hubbard,
B.LaBombard, R.M.Churchill,T.Golfinopolous,
N.Tsujii, E.S.Marmar

September 2011

Plasma Science and Fusion Center
Massachusetts Institute of Technology
Cambridge MA 02139 USA

This work was supported by the U.S. Department of Energy, Grant No. DE-FC02-99ER54512.

Scaling of H-mode threshold power and L-H edge conditions with favorable ion grad-B drift in Alcator C-Mod tokamak

Y.Ma, J.W.Hughes, A.E.Hubbard, B.LaBombard, R.M.Churchill,T.Golfinopolous, N.Tsujii, E.S.Marmar, *MIT PSFC*

Massachusetts Institute of Technology, Plasma Science and Fusion center
175 Albany Street, Cambridge, MA 02139 USA

Abstract

The low-to-high confinement transition (L-H) has been systematically studied in Alcator C-Mod lower single null (favorable ion grad-B drift) plasmas, covering an extensive global plasma parameter space. Plasma density ($\overline{n}_e$), toroidal magnetic field strength (B_T), and plasma current (I_p) dependence of H-mode threshold power (P_{th}) and local plasma edge conditions are investigated. The P_{th} dependence on density is nonlinear and has a "U-shape", which is not sensitive to plasma current variation, and affected by B_T mainly in low densities. The L-H local edge conditions, including the amplitude and gradient scale length of T_e, n_e profiles, are evaluated at times just before L-H and at two radial locations: ρ=0.95 and ρ=1.0. The behavior of edge conditions at the two locations exhibit a number of major differences in terms of their scaling with global parameters. In all, the scaling of L-H P_{th} and edge conditions are complex, neither of which can be simply represented by a relation of the type $\overline{n}_e{}^x B_T{}^y I_p{}^z$. Local parameters are also evaluated in low power L-mode and compared with the L-H companion. Noticeable differences between L-mode and L-H are mainly observed in T_e at ρ=0.95 and L_n, L_T near separatrix, while other parameters are found to be not significantly changed. Comparison with resistive-ballooning mode theory yield reasonable good agreement, such that the experimental data at ρ=0.95 fit into the corresponding L-mode and H-mode domains, as well as L-H boundary predicted by theory. A period of improved energy confinement similar to I-mode is identified in a few low density 5.4T discharges prior to L-H transition.

1. Introduction

Since the first experimental demonstration of H-mode [1], the low-to-high confinement transition (L-H) studies have attracted considerable research efforts: not only the transition physics per se is of great interest, but also because this subject is closely related to the important issue of predicting required threshold power for H-mode access (P_{th}), which is a critical engineering parameter in the design of new tokamaks, e.g. ITER. Early studies were focused on assembling data of P_{th} from multiple devices into a database and extracting an empirical scaling law with global plasma parameters out of it. These works yielded the international tokamak scaling [2]:

$$P_{th}\,[MW]=0.049\,\bar{n}_e\,[10^{20}m^{-3}]^{0.72}B_T[T]^{0.8}S[m^2]^{0.94}$$

, which indicates that the three primary dependencies of P_{th} are plasma density, strength of toroidal magnetic field, and plasma surface area. Large departures from the scaling law prediction have been constantly discovered: one is the 'U-shape'-like non-monotonic density scaling seen on several devices (e.g. AUG [3], JET [4], also C-mod [5] as shown later in this paper), where magnitudes of P_{th} were found to substantially increase below a threshold density, and demonstrate significant divergence from the scaling law. This low density regime has become a concern for ITER, since if ITER is operated there, the scaling law based target design of its required auxiliary heating capability might be insufficient to ensure H-mode access. As a consequence, using the scaling law as a first principle predicting tool may not be reliable enough; the importance of understanding the underlying physics needs to be invoked.

Compared with P_{th}, threshold plasma edge conditions are considered to be more directly and closely related to L-H physics, hence a comprehensive characterization of them could yield more phenomenological understanding of L-H onset and provide some guidance to experiments. Besides, studying the edge conditions could also help identify the potential L-H 'critical parameters' and test their validity. For example, $T_{e,95}$, the electron temperature in plasma edge, has been considered as the critical condition for L-H transition and widely investigated in the past. Some earlier works [6][7][8] suggest that $T_{e,95}$ is generally a good metric: magnitudes in L-mode are distinguishably lower than in H-mode plasmas, and the two domains are usually seen to be clearly divided by the L-H threshold boundary. The dependence of L-H threshold $T_{e,95}$ on global plasma parameters, e.g. $\bar{n}_e$, B_T, and I_p was studied in these works via regression analysis, which led to power law based scaling of the type $T_{e,95}\sim\bar{n}_e^{\,x}\,B_T^{\,y}\,I_p^{\,z}$. Another important reason for studying threshold plasma conditions is that they can either be directly compared with, or to be used as input variables to test various theoretical models proposed for L-H transition. These comparisons can improve the understanding of the physical mechanism that triggers L-H.

The core of this paper is to examine the plasma density, B_T, and I_p dependence of P_{th} and local plasma edge conditions in standard Alcator C-Mod lower single null plasmas in a broad global parameter space, which will be the themes of section 3 and section 4. Section 2 will briefly discuss experimental conditions and data analysis techniques;

section 5 will show results from the comparisons between resistive-ballooning mode theory and experiments; section 6 will demonstrate the existence of improved energy confinement prior to L-H transition in low density plasmas; section 7 includes conclusions and future work.

2. Experimental description and data analysis

2.1. Experimental description

The discharges included in this study are all deuterium plasmas and originate from dedicated L-H transition or H-mode pedestal experiments between 2005 and 2010 C-mod experimental campaigns. This large set spans a wide variation of global plasma conditions: line averaged plasma density ($\overline{n}_e$) between 0.6 x10^{20}m^{-3} and 2.5 x10^{20}m^{-3}, toroidal magnetic fields (B_T) from 3.5T and 5.4T, and plasma currents (I_p) ranging from 0.6MA to 1.4MA. Equilibrium magnetic configurations for these discharges are maintained to be nearly fixed, with κ ~1.7, δ_{upper} ~0.35, δ_{lower} ~0.5. All these plasmas were created in lower single null configuration, with ion grad-B drift in the favorable direction for H-mode access. Most low density ($\overline{n}_e$ <1.0 x10^{20}m^{-3}) plasmas in the set originate from two dedicated L-H transition experiments: one conducted in B_T =5.4T plasmas during 2007 C-mod campaign (later, data from this experiment are displayed in different symbols in order to be distinguished from other 5.4T data), the other one in 2008 campaign with B_T / I_p operated at 3.5T/0.6MA. In addition to density variation, plasma currents were also scanned at three values (0.6,0.9,1.2MA) in the 2007 experiment. Cryopump, as demanded, was utilized in low density experiment to provide better plasma density control and reduce the edge fuelling sources.

In most scenarios, Ohmic power alone is not sufficient to induce L-H transition. For all quoted discharges, L-H confinement bifurcations were obtained by applying auxiliary heating power, which is solely ICRF, during B_T and I_p flattops, i.e. periods in which neither B_T or I_p is significantly varied. ICRF antenna frequency on C-Mod can be adjusted between 40 and 80MHz, and was tuned at the value according to the specific operational B_T to perform on-axis hydrogen fundamental minority heating. Input ICRF power was added in a slow continuous ramp-up pattern, providing a broad range of input power which covers the L-H threshold.

A defined L-H transition is usually discerned by the simultaneous occurrence of the following experimental evidence: an abrupt sharp drop of divertor D_α emission, a clear break-in-slope rise of line averaged density and confined plasma energy, an enhanced burst of edge electron temperature, and a suppression of plasma turbulence. Accessed H-mode plasmas exhibit prompt formation of both edge temperature and density pedestals following L-H transition. Time histories of some key plasma parameters resolving a typical L-H transition followed by a series of L-H-L transitions are shown by Fig.1.

2.2. Diagnostics and data analysis

Some key C-mod diagnostics are needed to provide relevant measurements. Among them, the Thomson scattering (TS) system [9] operated with up to two Nd:YAG lasers each at 30Hz and pulsed alternatively is used as the chief diagnostic for electron temperature (T_e) and density (n_e) measurements along a vertical chord through the magnetic axis. The spatial resolution of TS measured profiles, when mapped to midplane, is ~cm in plasma core and 1~2mm in the plasma edge. Electron cyclotron emission (ECE) diagnostics provide sub ms midplane electron temperature measurements at reduced spatial resolution. Line integrated plasma density is recorded by a multi-chord two-color CW interferometer system. Phase contrast imaging (PCI) and magnetic pick-up coils are used to monitor plasma density and magnetic fluctuations, respectively. For a limited number of discharges, edge impurity (boron) ion temperature (T_I) is measured by B^{5+} charge exchange recombination spectroscopy. Illustration of measurement locations for these diagnostics relative to a cut of C-Mod poloidal cross section is shown by Fig.2.

The TS measured T_e and n_e are mapped to the midplane using the equilibrium reconstruction code EFIT [10]. Then these mapped measurements, combined with the T_e data collected by ECE and evaluated at the corresponding TS time slices, are fitted into smooth curves to generate global radial profiles of T_e and n_e. The edge data, referred to those with $r>a_0$-2cm, are fitted utilizing the modified *tanh* function as defined in [11]. Typical examples of edge TS measurements and profile fitting are represented by Fig.3. The included data originate from the last two TS laser pulses before an L-H transition. This figure shows the case of both a high density ($\overline{n}_e$ ~1.8 x10^{20}m^{-3}) and a low density ($\overline{n}_e$ ~0.8 x10^{20}m^{-3}) discharge, which is a stringent test for the quality of TS data and profile fitting because of the low *S/N*. Although the measurement uncertainties can be larger compared with cases of higher densities, the profile fitting is still quite reliable.

The EFIT returned separatrix radial locations have been routinely used, which for most cases are seen to be reasonably accurate. The uncertainties from EFIT separatrix findings are usually of a few *mm*, thus the induced data scatters need to be taken into account and reduced. In the following sections, the profiles for each included discharges are shifted in the radial direction, so that the EFIT separatrix is aligned with the location of maximum d^2P_e/dr^2, which is nearly the pedestal foot of electron pressure ($P_e = n_e\ T_e$) profile in the sense of modified *tanh* function [11]. The required adjustments are seen to be generally minor for most cases, which are found to be within 3*mm*. We examined that the general trends discussed in the following sections are not changed by such small shifts. Another approach employed in this study to reduce data scatter is averaging data over a finite radial extent, and using the mean values within the entire region in the evaluation. This method will be employed later (section 4, 5) in assessing local edge plasma conditions, specifically the profile gradient scale lengths.

3. H-mode threshold power

H-mode threshold power is characterized by the total power loss to the plasma boundary, which is defined according to [2] as:

$$P_{th}=P_{tot}-dW/dt=P_{OH}+P_{aux}-dW/dt$$

, and assessed at L-H transition times. In the above definition, P_{OH} is the Ohmic heating power and dW/dt is the time derivative of plasma stored energy, both are calculated using the EFIT code. ICRF is the sole auxiliary heating source employed in this study, so in this case $P_{aux}=cP_{RF}$, where P_{RF} is the net input ICRF power measured by waveguide couplers, and a numerical factor c is multiplied to account for the fractional absorption of ICRF power by plasmas. Measured minority ion density concentrations relative to main ion (n_H/n_D) for most quoted discharges were about 5%-10%, which is efficient for single pass ICRF power absorption in the hydrogen minority heating scenario [12]. Accurately knowing the value of c requires dedicated numerical ICRF wave simulation, which is beyond the scope of this study. Some earlier studies [12] proposed a reasonable estimate of c based on ECE break-in-slope measurements to be about 90% in normal C-mod discharge conditions. For simplicity, we make the assumption that ICRF power launched by antennas are 100% absorbed, thus c=1.0 and $P_{tot}=P_{OH}+P_{RF}$. The difference between assuming c=1.0 and c=0.9 can induce some minor discrepancies (<0.3MW) in calculating P_{th}, but will not change the general conclusions. The net power loss, $P_{net}=P_{th}-P_{rad,main}$ may be a more appropriate quantity to characterize the H-mode threshold power. Upon an examination, the $P_{rad,main}$ for the included discharges are mostly about 0.3MW and essentially independent of density. So the overall trend of P_{net} is basically differed from that of P_{th} by an offset.

As shown in Fig.4, P_{th} in 5.4T exhibits a clear 'U-shape', which decreases monotonically with density for $\overline{n}_e$<1.0x10^{20}m^{-3}, while it increases with density for $\overline{n}_e$>1.8x10^{20}m^{-3}. In the broad range between the two limits, the P_{th} exhibits a local minimum, which is close to 1.5MW and basically invariant with density. The same behavior of P_{th} in the low density regime ($\overline{n}_e$<1.0x10^{20}m^{-3}) was also reported in a dedicated study of the 2007 experiment [5]. The overall trend with $\overline{n}_e$ can be nearly represented by a simple analytical function of $1.5/\overline{n}_e^{\,2}+0.2\,\overline{n}_e^{\,3.5}$, as shown by the dashed curve on Fig.4. Predictions from the international tokamak scaling (solid line, with B_T =5.4T, S~7.5m^2) are compared, which is seen to deviate from experimental data at most places, especially for $\overline{n}_e$<1.0x10^{20}m^{-3} and $\overline{n}_e$>2.0x10^{20}m^{-3}, where the scaling law prediction seem to be much lower. Moreover, the plasma density dependence suggested by the scaling law is nearly linear ($\sim\overline{n}_e^{\,0.7}$), which is completely different than the experimental observation. Although I_p is varied by a factor of 2 in these discharges, data of P_{th} exhibit no clear I_p dependence in the range of 0.6x10^{20}m^{-3}< $\overline{n}_e$ <2.2x10^{20}m^{-3}. It means that P_{th} is better correlated with plasma density, rather than normalized Greenwald fraction $\overline{n}_e/n_G$, where n_G [10^{20}m^{-3}]= I_p [MA]/(π a_0[m]^2) is the Greenwald density. In absence of sufficient data, I_p dependence for $\overline{n}_e$>2.2x10^{20}m^{-3} is unknown. As previously noted, a similar 'U-shape' dependence of P_{th} on density has also been observed on many devices, e.g. AUG[3], JET[4], etc, suggesting that this feature might be universal, although the values of density at minimum P_{th} differ, and the underlying physics for these are still not well understood.

To reveal the role played by toroidal magnetic field (B_T), data from lower B_T (3.5T, 4.6T) discharges are shown together with portions (I_p=0.6-1.0MA) of 5.4T data on Fig.5. The B_T dependence of P_{th} is mainly seen at low density of $\overline{n}_e$ <0.9x10^{20}m^{-3}, where for fixed $\overline{n}_e$, values of P_{th} in lower B_T are noticeably smaller. However, as $\overline{n}_e$ is increased above 1.0 x10^{20}m^{-3}, values of P_{th} from various B_T at a certain $\overline{n}_e$ are seen to be close, which suggest that the B_T dependence diminishes or may even vanish at higher density. The overall density scaling tend to remain 'U-shape' in lower B_T, however, owing to the existence of B_T effects, the enhancement of P_{th} in low densities becomes less pronounced. An approximate curve fitting of 3.5T data is shown by the green dashed line in Fig.5. Comparing with the 5.4T one (black dashed line) suggests that the density at minimum P_{th} varies with B_T. For B_T>6.0T, the fundamental hydrogen minority heating scenario can not be realized in C-Mod plasmas. To avoid confusion in data interpretation induced by the discrepancies in heating schemes, those data are not included for comparison. Therefore, the density scaling of P_{th} in high B_T (B_T >5.4T) plasmas remains unknown.

In all, the above experimental evidence suggests that the density and B_T dependence of P_{th} can not be described by a simple relation of the type $\overline{n}_e^{\,x}\, B_T^{\,y}$. There are indication that the correlations with the two variables ($\overline{n}_e$,B_T) can be convoluted, for example, the specific B_T dependence varies with density as already seen. The poor agreement between the scaling law predictions and experimental results reinforce the importance of understanding L-H edge conditions and their relations with H-mode threshold power, eventually aiming at a physics-based reliable prediction capability.

4. Edge plasma conditions

Compared with global threshold power, which could be influenced by many physical and engineering factors (e.g. RF power absorption efficiency, neutrals, wall conditions, energy confinement, etc), plasma conditions either in the edge or scrape-off layer (SOL) region are expected to be more relevant to L-H physics. In this section, characterization of local edge conditions and their scaling with $\overline{n}_e$, I_p and B_T are examined both near L-H threshold and in low power L-mode, in order to improve the understanding of the local criteria achieved at (perhaps also required for) L-H transition, and to provide inputs to test various proposed models.

The edge plasma conditions near L-H threshold (still in L-mode) are examined in 4.1 and 4.2. The evaluation is performed in the same set of discharges involved before, using the T_e and n_e profiles obtained by fitting into the data from the last two TS pulses prior to L-H, and radially shifted according to the criteria stated earlier in section 2. The edge conditions are assessed at two radial locations of ρ=0.95, which is approximately at a_0-8*mm* in minor radius, and ρ=1.0, which is the EFIT separatrix, or equivalently the P_e "pedestal foot" after the alignment. Here, ρ is the normalized poloidal flux.

Parameters employed to characterize the local T_e and n_e profile shapes are their gradient scale length, normalized to midplane plasma minor radius a_0, i.e., $a_0/L_T=(a_0/T_e)dT_e/dr$ and $a_0/L_n=(a_0/n_e)dn_e/dr$. Amplitudes of a_0/L_T and a_0/L_n are seen to increase substantially in the narrow region between ρ=0.95 ($r\sim a_0$-8mm) and ρ=1.0, as seen from Fig.6.d-e. To reduce data scatter, the means of a_0/L_T and a_0/L_n within the two shaded areas (see Fig.6) are used as the values for ρ=0.95 and ρ=1.0, respectively. Local conditions of T_e and n_e are assessed at the two specific locations, which are marked by the two dashed lines in Fig.6. All data are displayed against the $\overline{n}_e$ evaluated at the corresponding L-H times for each discharge. The error bars shown on some data in Fig.7-10 are estimated utilizing the Monte Carlo profile error analysis technique [13].

Before a detailed examination of the parametric dependence of L-H threshold local edge conditions, some edge profiles are assembled and displayed together in Fig.6 to provide an intuitive sense. Plasmas of the demonstrated profiles cover a parameter space of 2 plasma densities ($\overline{n}_e\sim0.7\text{x}10^{20}\text{m}^{-3}$, $1.0\text{x}10^{20}\text{m}^{-3}$), 2 values of B_T (B_T=3.5T, 5.4T), and 3 plasma currents (I_p=0.6, 0.9, 1.2MA). Some features are clearly exhibited by these plots, for example, with similar plasma density (say $\overline{n}_e\sim1.0\text{x}10^{20}\text{m}^{-3}$), near separatrix T_e profiles are maintained approximately identical in shape (see plot of a_0/L_T). Progressing radially inward to ρ=0.95, we see that T_e profiles with different I_p (at similar density and B_T) clearly diverge, such that the one with higher I_p becomes much steeper (correspond to larger a_0/L_T), hence I_p dependence of T_e gradient scale lengths emerge at this location. These observations are also verified below in 4.1 and 4.2, where more characteristics of L-H edge conditions will be demonstrated.

4.1. L-H local conditions at ρ=0.95

We start the discussion with focus a on 5.4T data to examine plasma density and I_p dependence of $T_{e,95}$ and $P_{e,95}$ (T_e and P_e at ρ=0.95) at L-H threshold. First, remarkable enhancement of $T_{e,95}$ is clearly identified in low densities ($\overline{n}_e<1.0\text{ x}10^{20}\text{m}^{-3}$), as shown by Fig.7.a, the manifested trend can be nearly represented by $\sim1/\overline{n}_e$ relation. Recall this is also the density range where H-mode P_{th} exhibit a strong inverse density scaling ($\sim1/\overline{n}_e^{\,2}$) as seen before. However, the $\sim1/\overline{n}_e$ dependence of $T_{e,95}$ is not obeyed in moderate ($1.0\text{x}10^{20}\text{m}^{-3}<\overline{n}_e<1.8\text{x}10^{20}\text{m}^{-3}$) and high ($\overline{n}_e>1.8\text{x}10^{20}\text{m}^{-3}$) densities, where we found values of T_e generally scatter between 100-200eV and exhibit no clear trends with $\overline{n}_e$. The observed characters of $T_{e,95}$ at $\overline{n}_e>1.0\text{x}10^{20}\text{m}^{-3}$ are consistent with the result from earlier studies on C-Mod [8], however, the low density branch was not extensively covered in that work. Because $n_{e,95}$ is well (essentially linearly) correlated with $\overline{n}_e$ (Fig.7.b), values of $P_{e,95}$ (Fig.7.c) in the range of $\overline{n}_e<1.5\text{x}10^{20}\text{m}^{-3}$ are maintained close to $0.1eV\text{x}10^{20}m^{-3}$, and only exhibit slight variation with density; however, for $\overline{n}_e>1.5\text{x}10^{20}\text{m}^{-3}$, data of $P_{e,95}$ manifest a clear prompt rise with density. No clear I_p dependence has been identified in T_e, n_e, or P_e at ρ=0.95.

In Fig.8, data from two lower toroidal fields of B_T=3.5T and B_T=4.6T are assembled and shown together with portions of 5.4T data to demonstrate the B_T dependence. We assume that the absence of I_p dependence on T_e and P_e derived from 5.4T data is valid independent of the strength of B_T. With this assumption, the B_T dependence of T_e, n_e, and P_e are investigated by comparing data with different B_T at similar densities.

The same linear correlation of $n_{e,95}$ with $\overline{n}_e$ previously observed in 5.4T data is also followed in cases of lower B_T. It means that $n_{e,95}$ is primarily correlated with $\overline{n}_e$, and insensitive to either I_p or B_T variation. Later it will be shown in 4.2 that this conclusion is also true near the separatrix. The B_T dependence of $T_{e,95}$ (Fig.8.a) is more complicated. It is first noticed that for $\overline{n}_e$<0.9x10^{20}m^{-3} and at fixed $\overline{n}_e$, values of $T_{e,95}$ in lower B_T (e.g. 3.5T) plasmas are reduced. As $\overline{n}_e$ increases above 1.0x10^{20}m^{-3}, $T_{e,95}$ is found to be insensitive to B_T, such that ranges covered by data of different B_T basically overlap. Consequently, the overall density scaling of $T_{e,95}$ is affected by B_T variation: the clear ~1/ $\overline{n}_e$ scaling of $T_{e,95}$ at low density as identified from 5.4T discharges become ambiguous in 3.5T; rather, most 3.5T data as seen are scattered between 100eV and 200eV without showing apparent variation with plasma density. Prior studies done in C-Mod moderate-density ($\overline{n}_e$ ~1.5x10^{20}m^{-3}) 8T plasmas [14] suggest a remarkable enhancement of $T_{e,95}$ compared to 5.4T. This observation casts more questions on the behavior of $T_{e,95}$ at L-H threshold, which can not be fully answered by this study and requires further investigation. Taken together, these evidence indicate that similar to the circumstance of P_{th}, the plasma density and/or B_T dependence of $T_{e,95}$ can not be simply described by any relation of the type $\overline{n}_e^{\,x}\, B_T^{\,y}$ over an extensive global parameter space.

Fig.9.a-b shows the density scaling of T_e and n_e scale lengths in 5.4T plasmas at ρ=*0.95*. These plots reveal a notable separation of data with different I_p in both L_T and L_n at fixed density, a feature not seen in either T_e or n_e as shown before. For most included data, the magnitudes of a_0/L_T (Fig.9.a) are found to be approximately proportional to I_p. However, for a_0/L_n (Fig.9.b), this proportionality (~I_p) seems to be mainly identified at $\overline{n}_e$<1.0x10^{20}m^{-3}. At higher density of $\overline{n}_e$>1.0x10^{20}m^{-3}, I_p dependence of a_0/L_n tends to be weak or may even vanish. Owing to the existence of I_p effects, dependence of a_0/L_T and a_0/L_n on plasma density can only be examined for some fixed values or a narrow range of plasma currents. Since large portions of I_p on the plots are concentrated in 0.8MA<I_p<1.0MA, we choose to utilize data with I_p within this range to elucidate the density dependence. These data suggest a weak inverse correlation of a_0/L_T with $\overline{n}_e$, even for $\overline{n}_e$<1.0x10^{20}m^{-3}, where $T_{e,95}$ increase considerably. Therefore at ρ =0.95 with fixed I_p, shapes of T_e profiles (i.e., L_T) at L-H seem to be relatively resilient to plasma density variation and maintained similar; I_p, as indicated, is one primary variable to determine T_e profile shape at ρ=0.95. Values of a_0/L_n at fixed I_p are found to be close to constant at low density, and decrease monotonically at moderate and high density.

Investigation of B_T effects on local gradient scale lengths are performed between data of *3.5T/0.6MA* and *5.4T/0.6MA*. Results are presented in Fig.10. The comparisons have to

be restricted between data with similar I_p, since it is already known from earlier discussion that gradient scale lengths were highly dependent on I_p. Similar to that in $T_{e,95}$, distinguishable dependence of B_T on both a_0/L_T and a_0/L_n are observed at low density of $\overline{n}_e$<1.0x10^{20}m^{-3}. Combined with the previously identified ~I_p proportionality, it suggests that a_0/L_T and a_0/L_n at ρ=0.95 could correlate with q_{95} (q_{95}~a_0B_T/R_0I_p) at low density. In Fig.11, data of $\overline{n}_e$<0.9x10^{20}m^{-3} with various I_p and B_T are displayed versus q_{95}, which reveals that a_0/L_T, a_0/L_n ~$1/q_{95}$. Dependence of a_0/L_T and a_0/L_n on B_T is weak at higher densities of 1.0x10^{20}m^{-3}< $\overline{n}_e$<1.5x10^{20}m^{-3}, and not clear for $\overline{n}_e$>1.5x10^{20}m^{-3} due to the lack of sufficient 3.5T data.

4.2. L-H local conditions near separatrix

Local conditions near the separatrix, or equivalently the P_e "pedestal foot" after applying the alignment criteria (see 2.2), are shown by companion with those at ρ=0.95 to highlight similarities and differences in the global scaling between the two locations. Since the nominal lower bound on reliable TS measurements is ~3x10^{19}m^{-3} [9], only data with local n_e above this value are included. A glance at Fig.7.d-f and Fig.8.d-f reveals an absence of distinguishable I_p or B_T dependence on separatrix T_e and n_e. Hence attention is mainly concentrated on the overall plasma density dependence manifested by all data.

First we see values of $T_{e,sep}$ as shown by Fig.7.d are mainly restricted in the range between 50eV and 100eV, which are consistent with the expectation from the two-point divertor power balance model [15]. The variation of $T_{e,sep}$ with density is weak, therefore the significant enhancement of $T_{e,95}$ in low density 5.4T plasmas should not be attributed to a significant elevation of boundary condition, $T_{e,sep}$. Later, it will be shown that this is more associated with the alteration of near-separatrix T_e profile shapes, that is, the appearance of a mild T_e pedestal. A difference between $n_{e,sep}$ and $n_{e,95}$ is that data of $n_{e,sep}$ at $\overline{n}_e$>1.5x10^{20}m^{-3} clearly diverge from the linear trend obtained from $\overline{n}_e$<1.5x10^{20}m^{-3}, whereas a linear scaling was seen to well represent the data trend for $n_{e,95}$ over the entire density range. Suggested by Fig.7.e, the trend of $n_{e,sep}$ at high density can be nearly represented by a ~$\overline{n}_e^{\,3.0}$ relation.

Characterizations of local gradient scale lengths near separatrix are illustrated by Fig.9.c-d and Fig.10.c-d. Unlike the case of ρ=0.95, either I_p no B_T effects on a_0/L_T could not be explicitly identified over the entire density range, yet a strong ~$1/\overline{n}_e$ overall correlation between a_0/L_T and density is clearly manifested. This evidence suggests that T_e profile shape (a_0/L_T) near separatrix is primarily sensitive to plasma density variation. Also, the strong increase of a_0/L_T at ρ=1.0 could be a main reason for the dramatic enhancement of $T_{e,95}$ in low densities at 5.4T, rather than $T_{e,sep}$, which is only slightly varied. In some very low density ($\overline{n}_e$<0.8 x10^{20}m^{-3}) plasmas with values of a_0/L_T near ρ=1.0 much exceeding those at ρ=0.95, even a mild T_e pedestal can form, e.g. the cases shown in yellow and green on Fig.6. Similar to a_0/L_T, apparent I_p dependence on a_0/L_n at ρ=1.0 is also absent. Dependence of a_0/L_n on plasma density at moderate and high density is demonstrated in Fig.9.d and Fig.10.d. Both figures show that a_0/L_n generally decreases with density. Unlike the case of a_0/L_T, the role of B_T on a_0/L_n is distinguishable: for fixed density, a_0/L_n

is reduced at lower B_T. Similar asymmetry was also observed previously between the B_T dependence of $T_{e,95}$ and $n_{e,95}$.

4.3. Relation with low power L-mode

Comparing edge conditions at L-H with those in low power L-mode (for simplicity, 'L-mode' in 4.3 and 4.4) is of particular importance in revealing what edge parameters are significantly changed during the course of plasma evolution from L-mode to L-H, and via what mechanisms these modification are achieved, which could further help identify the potential triggers for confinement bifurcation. Edge plasma conditions in L-mode are calculated in the same set of discharges involved in 4.1 and 4.2, using the T_e and n_e profiles obtained by fitting into the TS measurements within the first 50ms of I_p flattop for each discharge. The same spatial averaging of edge parameters used in section 4 is adopted. These data are mostly from Ohmic plasmas, but mixed with a small number of low-power (<0.5MW) ICRF ones.

Fig.12 reveals that L-mode $T_{e,95}$ are mainly scattered between 100eV and 200eV, and do not exhibit clear correlation with plasma density. Compared with $T_{e,95}$ at L-H, the values of L-mode $T_{e,95}$ (Fig.12.a) in most 5.4T plasmas are found to be lower. The divergence is especially clear for $\overline{n}_e$ <1.0 x10^{20}m^{-3}, where the data there suggest that significant increase of $T_{e,95}$ from the L-mode level is required in order to access H-mode. However, for most 3.5T and some 5.4T (those with moderate of 1.0x10^{20}m^{-3}<$\overline{n}_e$<1.5x10^{20}m^{-3}, i.e. near the minimum of P_{th}) plasmas, the values of $T_{e,95}$ in L-mode and at L-H are seen to be comparable, which could suggest that $T_{e,95}$ in these cases might not very likely be the "critical" parameter need to be achieved for L-H transition. Unlike $T_{e,95}$, the $n_{e,95}$, $T_{e,sep}$ and $n_{e,sep}$ in L-mode are not dramatically different than L-H. The values of a_0/L_T and a_0/L_n at ρ=1.0 (Fig.13.a-b) in L-mode are generally lower than what they are at L-H. By contrast, data of both L_T and L_n at ρ=0.95 exhibit no significant overall divergence between L-mode and L-H.

4.4. Relation with SOL-divertor physics

As shown by Fig.14, the large scatters in data of a_0/L_T at ρ=0.95 for both L-mode and L-H induced by I_p and B_T variation can be reduced if these data are re-organized with respect to the dimensionless parameter $\overline{n}_e/n_G$. Reduced data scatter are also observed in $a_0/L_p = a_0/L_T + a_0/L_n$ over all densities since $a_0/L_T >> a_0/L_n$. The overall trend of a_0/L_T and a_0/L_p is basically the same: they generally increase towards lower values of $\overline{n}_e/n_G$, which are guided by the dash lines on Fig.14. Differences between L-mode and L-H could exist mainly in the high-recycling regime ($0.19<\overline{n}_e/n_G<0.31$), such that at fixed $\overline{n}_e/n_G$, values of a_0/L_p (also a_0/L_T) at L-H seem to be generally larger than in L-mode.

Early studies by LaBombard [16] discovered similar correlation between L_p and $\overline{n}_e/n_G$ in the near SOL ($a_0 < r < a_0 + 5mm$) region in Ohmic plasmas, and connect this feature with the potential role of electromagnetic drift wave turbulence on edge profile regulation.

Based on results shown in Fig.14, a similar scaling with $\overline{n}_e/n_G$ applies at ρ=0.95 for a_0/L_p (also a_0/L_T since $a_0/L_p \sim a_0/L_T$) in L-mode and at L-H. Curiously, the scale lengths at ρ=1.0 depend on $\overline{n}_e$, rather than the normalized Greenwald fraction. It is as if that at both ρ=0.95 and in the near SOL, plasma profiles are influenced by similar cross-field transport mechanism, and "pivoted" about the near separatrix location --an implication that the entire plasma edge and near SOL regimes should be studied as an integrated physical system.

5. Comparison with theory

A handful of theoretical models have been proposed in attempt to explain L-H transition, most of which can be found in the comprehensive review article by Connor and Wilson [17]. Rather than validating each of these models, we focus on testing a specific one based on a series of preceding works by Rogers, Drake and Zeiler (RDZ) [18][19][20]. This model relies on the suppression of resistive-ballooning mode turbulence as the mechanism for L-H transition. In this section, we aim at a comprehensive examination from experiment on the validity of RDZ model in predicting: (1) L-H transition threshold; (2) L-mode and H-mode operational domains. It is worthwhile to mention that similar comparisons were conducted before on Alcator C-Mod [8] in moderate densities, normal and high B_T (5T, 8T) plasmas, where encouraging agreement between theory and experiments have been found. Results shown below will extend this comparison into a broader parameter space, which covers a wide range of densities ($\overline{n}_e$=0.6-2.1 x10^{20}m^{-3}), three magnetic fields (B_T=3.5T, 4.6T, 5.4T), and more plasma currents (I_p=0.6-1.2MA).

The RDZ model indicates that the L-mode to H-mode confinement bifurcation is triggered when the critical conditions for suppressing resistive-ballooning mode instabilities induced particle and thermal transport are reached. The model relies on two dimensionless parameters to characterize mode stability and induced transport: the MHD ballooning parameter α_{MHD} ($\sim q^2 R d\beta/dr$), and the diamagnetic parameter α_{dia} ($\sim 1/\sqrt{q\upsilon_*}$, where $\upsilon_* \propto Z_{eff} q n_e / T_e^2$). Based on a number of three-dimensional nonlinear numerical simulations [18] performed previously in shifted-circle equilibrium magnetic geometry, an approximate L-H threshold boundary was obtained. As shown in Fig.15 by dashed lines, this boundary is in 'L' shape, with the two 'arms' being α_{MHD} ~0.5 and α_{dia}~0.6, respectively. H-modes are predicted to emerge in the space upper and right to the L-H boundary on the α_{MHD} - α_{dia} diagram, while L-mode are expected to stay in the remaining areas.

To experimentally examine the model predicted L-H threshold boundary, values of α_{MHD} and α_{dia} at L-H are evaluated for all discharges included earlier in this study at two radial locations of ρ=0.95 (Fig.15.a) and ρ=1.0 (Fig.15.c), staying in the same analysis scheme introduced in section 4. The assumption $T_e \sim T_i$ is applied here, thus $\alpha_{MHD} \sim 2\alpha_e$. This assumption is generally true in the high collisional C-Mod plasma edge, even at low

density, which is verified by the charge exchange T_i measurements. Same calculation are performed in low power L-mode (i.e., calculated from the first 50ms of I_p flattop, same as in 4.3) at ρ=0.95, and shown in Fig.15.b. It is noticed from Fig.15.a that the L-H data at ρ=0.95 are distributed close to the theory predicted boundary, which shows promising agreement. Compared with L-H, most data in low power L-mode are seen to be systematically lower in α_{MHD}, staying below the α_{MHD} =0.5. The increase of α_{MHD} is observed to be especially pronounced for α_{dia}~0.6. According to the results from 4.3, the enhancement of α_{MHD} (i.e. pressure gradients if I_p is fixed) are primarily achieved by the promotion of $T_{e,95}$, although in some cases, for example in the high-recycling regime, the increase of a_0/L_p (see Fig.14.c, Fig.14.f) may contribute as well. Also note that at ρ=0.95, the domain where low density data ($\overline{n}_e$ <1.0x10^{20}m^{-3} at L-H, open triangles on Fig.15.a) emerge on the diagram overlaps with that of the higher density ones, which implies that the local "bifurcation criteria" for L-H transition at different densities could be uniform, although the required heating power can vary strongly. Fig.15.d. shows that most L-mode and H-mode data largely appear in their corresponding domains as predicted by theory.

Although Fig.15.b suggests that the values of α_{dia} at ρ=0.95 in L-mode and at L-H are not remarkably different, the plasma evolution towards L-H, which is represented by the traces (those connected lines in Fig.16) on the α_{MHD} - α_{dia} diagram, could be different at various α_{dia}. We take three discharges with B_T =5.4T, I_p =0.8~1.0MA, at low ($\overline{n}_e$ =0.6 x10^{20}m^{-3}), intermediate ($\overline{n}_e$ =1.7 x10^{20}m^{-3}), and high ($\overline{n}_e$ =2.1 x10^{20}m^{-3}) density, to demonstrate the difference, as shown in Fig.16. Comparing the three plots, it is noticed that L-mode data in the low density (Fig.16.a) case mainly range between α_{dia}=1.0 and α_{dia}=2.0 as it progressively pass the L-H boundary of α_{MHD} =0.5. By contrast, in the intermediate density (Fig.16.b) case, the direction of the traces is essentially vertical towards the ideal MHD stability boundary for confinement bifurcation: α_{MHD} =1.0 [17], meanwhile remains closely aligned with α_{dia}=0.6 horizontally. Owing to its high collisionality, L-modes in the high density (Fig.16.c) case emerge in the region left to α_{dia}=0.6 and lower than α_{MHD} =0.5, so the direction of plasma evolution to L-H on the diagram is primarily upward right, which is a process of simultaneous promotion of α_{MHD} and α_{dia}. Interestingly, the scenario in the low density case is akin to the conditions required for nonlinear Kelvin-Holmholtz poloidal shear flow to be generated, sustained, and ultimately trigger L-H, that is α_{dia}~1.0, α_{MHD} <~0.5 [17][18].

Shown by Fig.15.c, data near separatrix (ρ=1.0) are mainly concentrated in the area lower and left relative to the predicted L-H threshold boundary on the α_{MHD} - α_{dia} diagram (i.e., α_{MHD} <0.5, α_{dia}<1.5), which is the result of higher collisonality (α_{dia}~$1/\upsilon_*$) and lower pressure near separatrix than ρ=0.95. So the resistive-ballooning mode turbulence near the separatrix might not be sufficiently suppressed to trigger L-H confinement bifurcation.

The above comparisons yield reasonably good agreements between theory and experiments, and have suggested a potential role of resistive-ballooning mode turbulence on L-H transition. However, these results provide no clues on the relation between the RDZ model and the observed edge conditions, e.g. $T_{e,95}$, or required H-mode threshold power. Neither can we directly prove the existence of resistive-ballooning mode until the

characters of edge fluctuations are well diagnosed and studied. Assessing the agreement between C-Mod data and other propose models is the subject of ongoing works.

6. Enhanced energy confinement before L-H at low density

In a few low density discharges ($\bar{n}_e$ ~0.6 x10^{20}m^{-3}, I_p=0.9MA, B_T=5.4T), an improved energy confinement phase was discovered before L-H transition. Time histories of some key plasma parameters for one such case are shown in Fig.17. This confinement phase share several common features with the I-mode regime [21], including (1) the appearance of substantial electromagnetic fluctuations in the intermediate frequency range with signature frequencies ~250KHz and detected by both magnetic pick-up coils and PCI; (2) steady and continuous improvement of plasma energy confinement indicated by H_{98} reaching H-mode level of above 1.0, but without clear H-mode transition during this course (L-H at 1.24 sec); (3) low edge neoclassical collisionality (see for example [21]), namely, $\upsilon_{*\,\mathrm{neo}}$~0.5; (4) appearance of a mild temperature (both T_e and T_I, see Fig.18) pedestal while the electron density profile retains an L-mode shape. Despite the low collisionality, Fig.18 indicates that electron and ion temperature in plasma edge are still well coupled, such that $T_e \sim T_I$.

Electron temperature and density profiles from the steady state period with well-established coherent fluctuations are compared with those in L-mode and H-mode, and shown by Fig.18. In general, T_e profile is similar to its H-mode companion but distinct with the one in L-mode: both support an edge pedestal, and the central T_e are comparable, which is 4~4.5*KeV*. The width of T_e pedestal (radial extension from pedestal top to bottom) is about 1.5cm, a little broader than that in the subsequent H-mode, which is about 1cm wide. Inside the pedestal, the two profiles are nearly identical. On the other hand, the density profile is found to remain in L-mode shape, perhaps slightly more peaked, but clearly without the formation of a steep density pedestal as in the H-mode scenario. Most of these properties are consistent with the typical I-mode profile characters, which have been described in [21].

Despite these similarities, this confinement phase differs from typical I-modes in certain aspects of first, these low-density discharges were created in standard lower single null magnetic topology (κ~1.66, δ_{upper}~0.35, δ_{lower} ~0.53) with ion grad-B drift in the favorable direction (i.e., pointing towards X-point), whereas most I-modes [21] are achieved either with unfavorable ion grad-B drift, or with favorable drift and atypical shaping. Because the H-mode threshold power is significantly enhanced at low density, an operation window exists for the enhanced confinement prior to H-mode transition. Similarly, I-mode access with unfavorable grad-B drift is allowed because P_{th} is much higher than in the favorable grad-B direction. There are two major differences between the intermediate frequency fluctuations (250*KHz* mode) and the commonly seen weakly coherent modes (WCM) in normal I-mode plasmas. One is that the bandwidth of the 250*KHz* mode is narrower (~30*KHz*) compared to those of WCM, which are typically 50~100*KHz* [21]. Another one is that the toroidal mode number, inferred by correlating

magnetic pick-up coils measurements at several different toroidal locations, is indicated to be low for the 250*KHz* mode, such that n<5; however, for standard WCM, n is typically above 10 [21].

Nevertheless, this confinement phase serves the same purpose as I-mode in combining the merit of H-mode on improving energy confinement, and of L-mode on maintaining right amount particle transport to avoid impurity accumulation.

7. Conclusion and future work

To summarize, plasma density, toroidal magnetic field strength, and plasma current dependence of H-mode threshold power (P_{th}) and local plasma edge conditions at L-H have been experimentally studied in Alcator C-Mod plasmas with favorable ion grad-B drift. Plasma density dependence of P_{th} was found to be 'U-shaped', which is similar to earlier observations on AUG, COMPASS, JET, JT-60, etc. Toroidal field dependence of P_{th} over the range of 3.5T<B_T<5.4T was found to depend on density: it is clearly identified at low density but becomes weak or may even vanish at moderate and high density. Despite a factor of 2 variations of plasma currents, no distinguishable I_p dependence of P_{th} was identified. For the few 5.4T discharges with lowest densities, an improved energy confinement emerged prior to L-H transition.

Local plasma edge conditions at L-H were characterized at two radial locations: ρ=0.95 and ρ=1.0 (near separatrix). At ρ=0.95, $T_{e,95}$ in 5.4T display a strong $\sim 1/\overline{n}_e$ scaling at low densities, while weak or no density dependence is found at high density. Effects of B_T on $T_{e,95}$ are mainly manifested at low density, such that for fixed $\overline{n}_e$, $T_{e,95}$ is lower for reduced B_T, however, the I_p dependence of $T_{e,95}$ is absent. It is found that $n_{e,95}$ is almost linearly correlated with plasma density, and is insensitive to either B_T or I_p variation. However, both I_p and B_T dependence were clearly identified in a_0/L_T and a_0/L_n, and it is likely that the proportionality is $\sim 1/q_{95}$ at low density. Near the separatrix, both $T_{e,sep}$ and $n_{e,sep}$ exhibit no I_p or B_T dependence. The density dependence of $T_{e,sep}$ is also weak even at low density; $n_{e,sep}$ diverge from linear scaling at high density. A strong $\sim 1/\overline{n}_e$ overall density scaling is identified in separatrix a_0/L_T, while both I_p and B_T dependence tend to be weak. The separatrix a_0/L_n is lower at reduced B_T, whereas I_p basically exerts no effect on separatrix a_0/L_n. Local conditions at L-H were also compared with those in low power L-mode, where distinct difference in the magnitudes of $T_{e,95}$ were found between the two cases in most 5.4T plasmas. Yet for moderate density 5.4T and most 3.5T plasmas, the values of $T_{e,95}$ in L-mode and at L-H are comparable. Amplitudes of a_0/L_T and a_0/L_n near separatrix at L-H seem to be larger than L-mode. Other parameters are not significantly different between the two cases.

Calculated local edge conditions have been used as inputs to test the resistive-ballooning mode theory (RDZ model). For ρ=0.95, data at L-H as shown on α_{MHD} -α_{dia} diagram are found to be distributed close to the theory predicted L-H boundary, while compared to L-H, values of α_{MHD} in L-mode seem to be systematically lower and well below the α_{MHD}

~0.5 boundary. In addition, data in L-mode and H-mode largely fall into their corresponding theory predicted domains on the diagram. Inside and near separatrix, data both in L-mode and at L-H are mostly scattered in the area of α_{MHD} <0.5 and α_{dia} <0.6, which is away from the theoretical boundary, and are not significantly changed from L-mode to L-H.

Future work will aim at better understanding of the physics of P_{th} and the correlation between P_{th} and local edge conditions, at resolving the evolution of edge conditions from L-mode to L-H in a finer time scale by employing improved time resolution diagnostics capability, at identifying the timing and triggers of L-H transition in various global plasma conditions, at looking for the differences and similarity between L-H and I-H transition, at searching for other major "hidden variables" in P_{th}, etc.

Acknowledgement

The authors wish to acknowledge J. Snipes for his experimental work at Alcator C-Mod on the low-density limit for H-mode access. This work was supported by US. Department of Energy Agreement DE-FC02-99ER54512.

References

[1] Wagner F, et al Phys. Rev. Lett. **53** 1453 (1982)
[2] Martin Y.R, Takizuka T, *et al.* , *Journal of Physics; Conference Series* **123** (2008) 012033
[3] Ryter F, et al., *Nucl Fusion* **49** (2009) 062003
[4] Andrew Y, *et al.*, *Plasma Phys Control Fusion* **48** (2006)
[5] Snipes J, *Proc 35th EPS Plasma Physics Conf.* (2008)
[6] Suttrop W, et al, Plasma Phys. Control. Fusion **39** 2051-2066 (1997)
[7] Righi E, et al, Plasma Phys. Control. Fusion **42** A199-A204 (2000)
[8] Hubbard A.E, et al, *Plasma Phys. Control. Fusion* **40** (1998)
[9] Hughes J.W, et al, Rev. Sci. Inst. 2003
[10] Lao L, et al, Nucl. Fusion
[11] Groebner R.J, et al, Nucl. Fusion 41 **12** (2001)
[12] Bonoli P, Fusion Science and Techonlogy, **51** pp.401
[13] Petty C.C, et al, Nucl. Fusion **38** 8 (1998)
[14] Hubbard A.E, et al, Phys. of Plasmas **14** 056109 (2007)
[15] Pitcher C.S, Stangeby P.C, Plasma Phys Control Fusion **39** (1997) 779-930
[16] LaBombard B, et al, Nucl. Fusion 45 1658 (2005)
[17] Connor J, *Plasma Phys. Control. Fusion,* **42** (2000) R1
[18] Rogers B, J.Drake, *Phys.Rev.Lett*., **79**(1997)
[19] Drake J F, et al, Phys. Rev. Lett. 77 494 (1996)
[20] Zeiler, Ph.D thesis, IPP report 1999
[21] Whyte D.G, *et al., Nucl Fusion,* **50**(2010) 105005

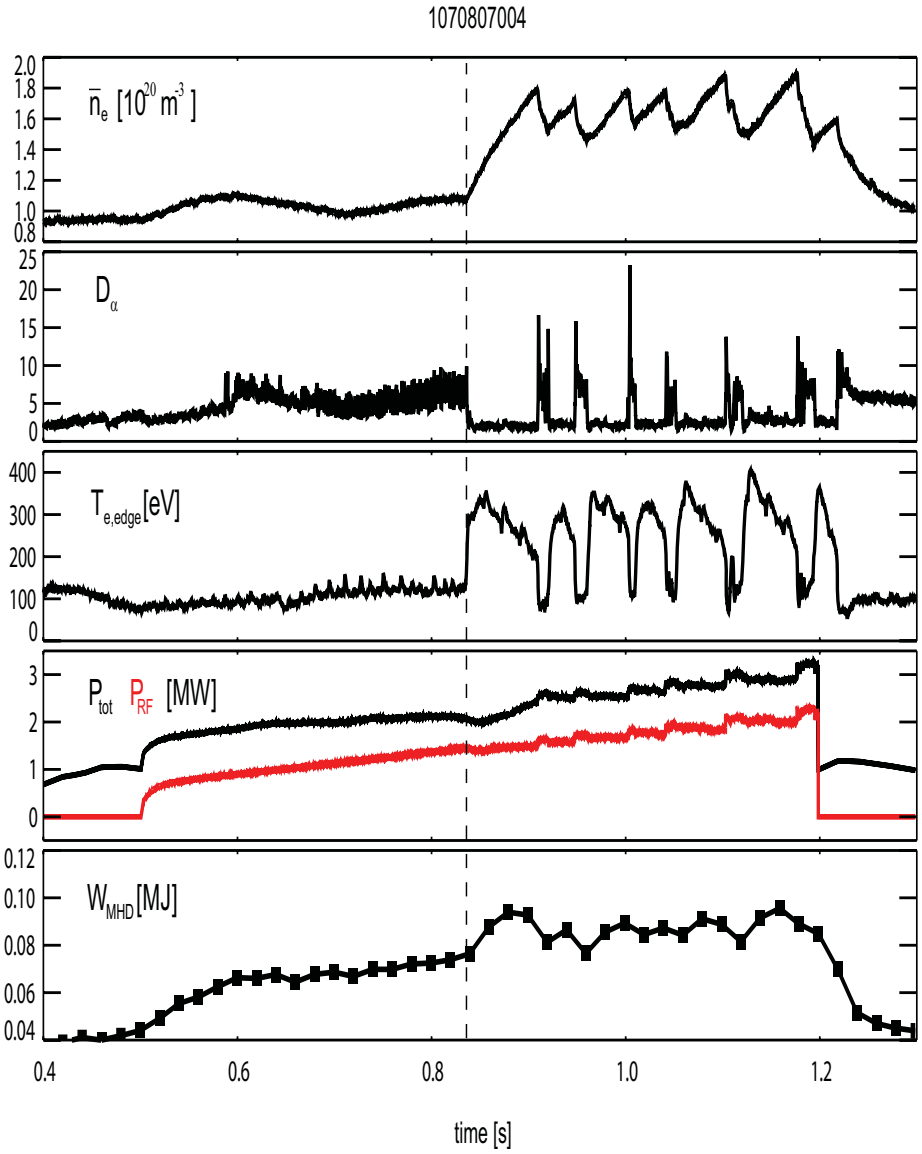

Fig.1. Time histories of some plasma parameters for a transition from L-mode to H-mode on C-Mod. The L-H transition is marked by the dashed line on these plots.

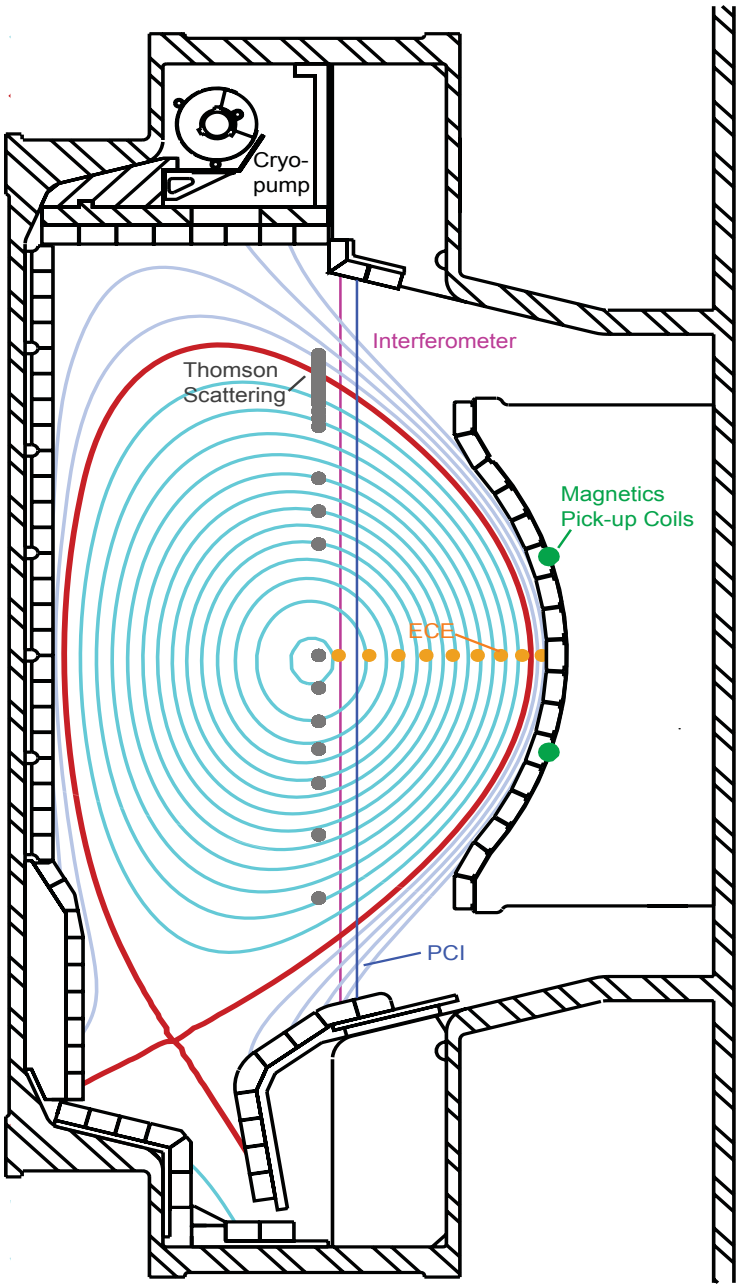

Fig.2. Illustration of standard lower single null equilibrium magnetic geometry on a poloidal cross section of Alctor C-Mod. Measurement locations of some key C-Mod diagnostics are displayed on the same plot.

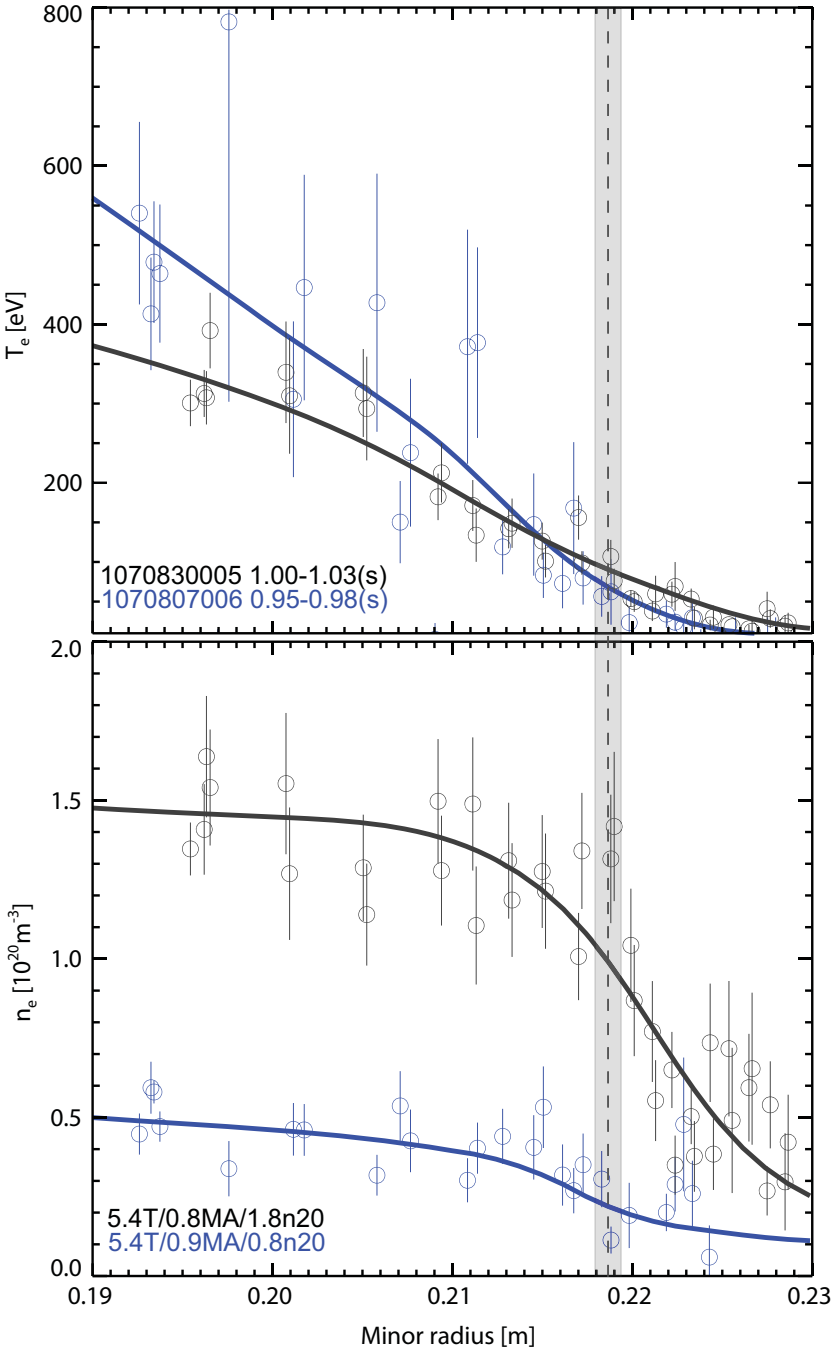

Fig.3. Thomson scattering measurements (open circles) of n_e and T_e in the edge region of a low ($\bar{n}_e$=0.8x10^{20}m^{-3}, blue) and moderate ($\bar{n}_e$=1.8x10^{20}m^{-3}, black) density discharge. The presented data are from the last two TS laser pulses, which is within ~30ms prior to L-H transition. Shown in solid lines are curve fitting to these data. The dashed line and shaded bar represent the approximate radial location of EFIT separatrix location.

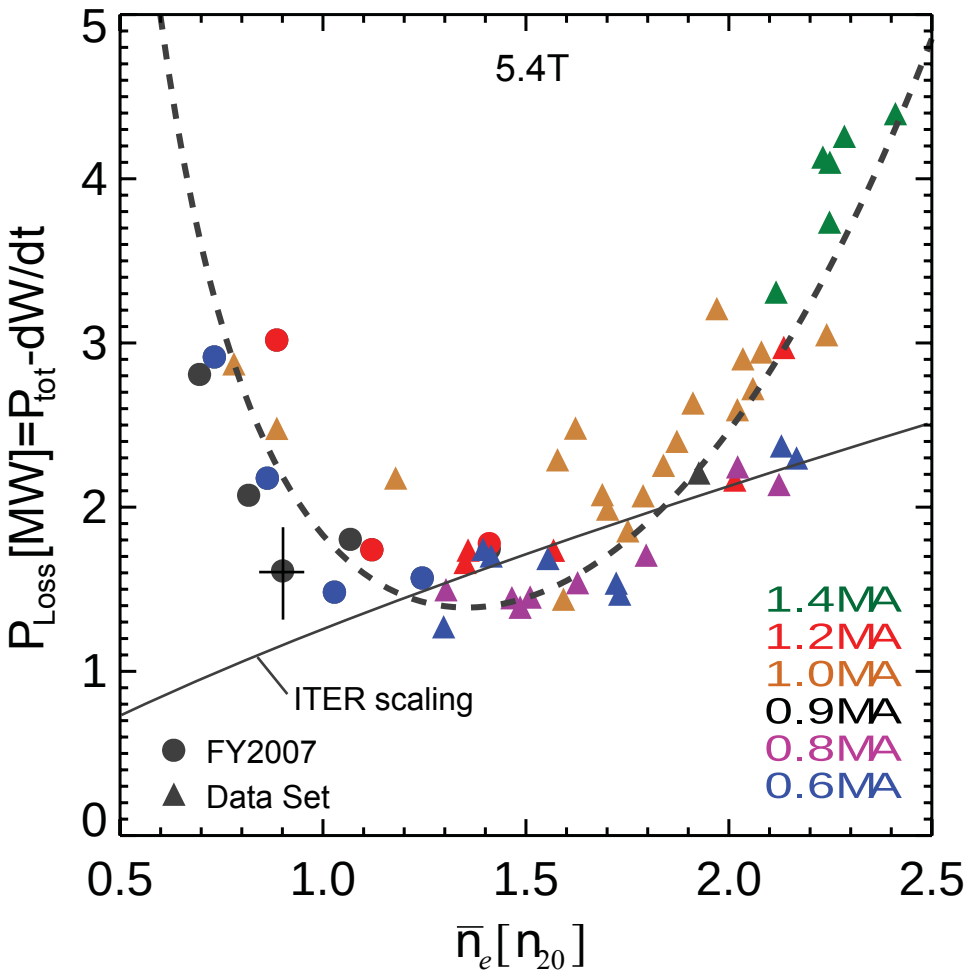

Fig.4. H-mode threshold power (P_{th}) in 5.4T plasmas versus line averaged density. Data from the dedicated low density L-H experiment in 2007 C-Mod campaign are shown by solid circles. Plot in dashed line is an approximate curve fitting to these data. The international tokamak scaling is shown as the solid line on the same plot.

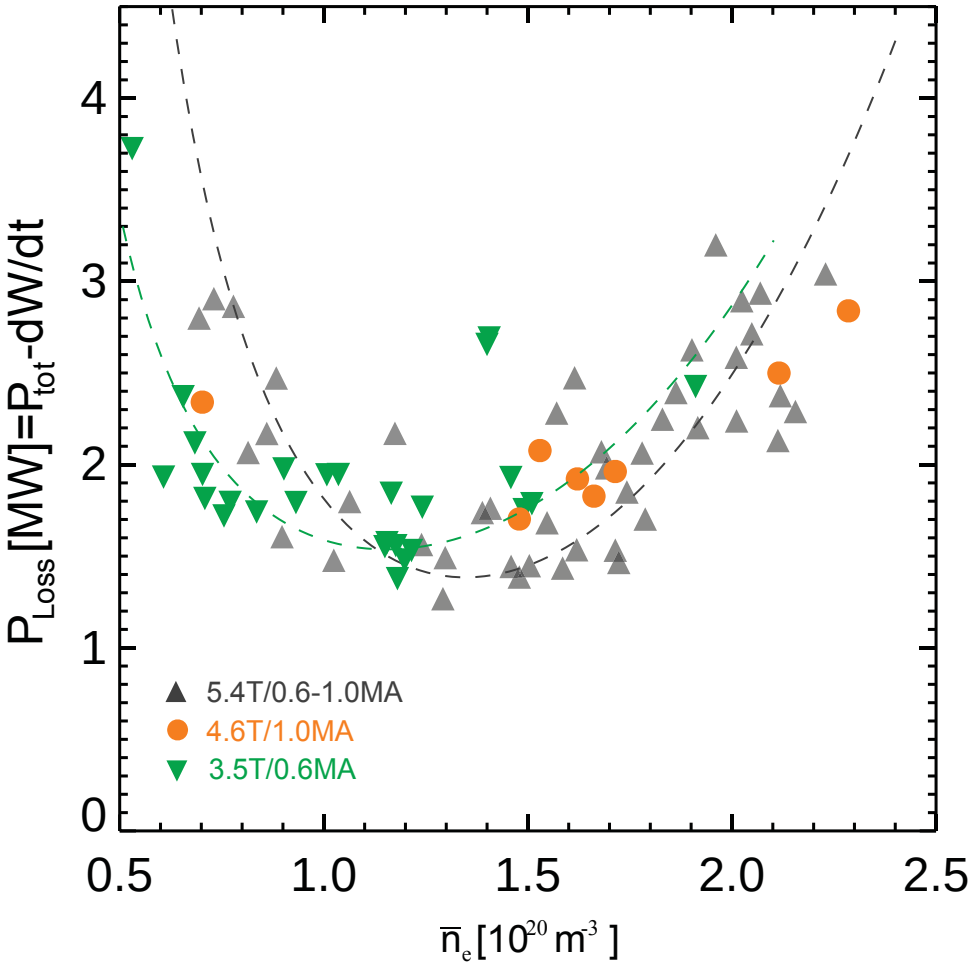

Fig.5. Data of P_{th} from lower B_T (3.5T, 4.6T) plasmas versus line averaged density are displayed together with portions of 5.4T data. The dashed line is the same curve fitting to 5.4T data as in Fig.4.

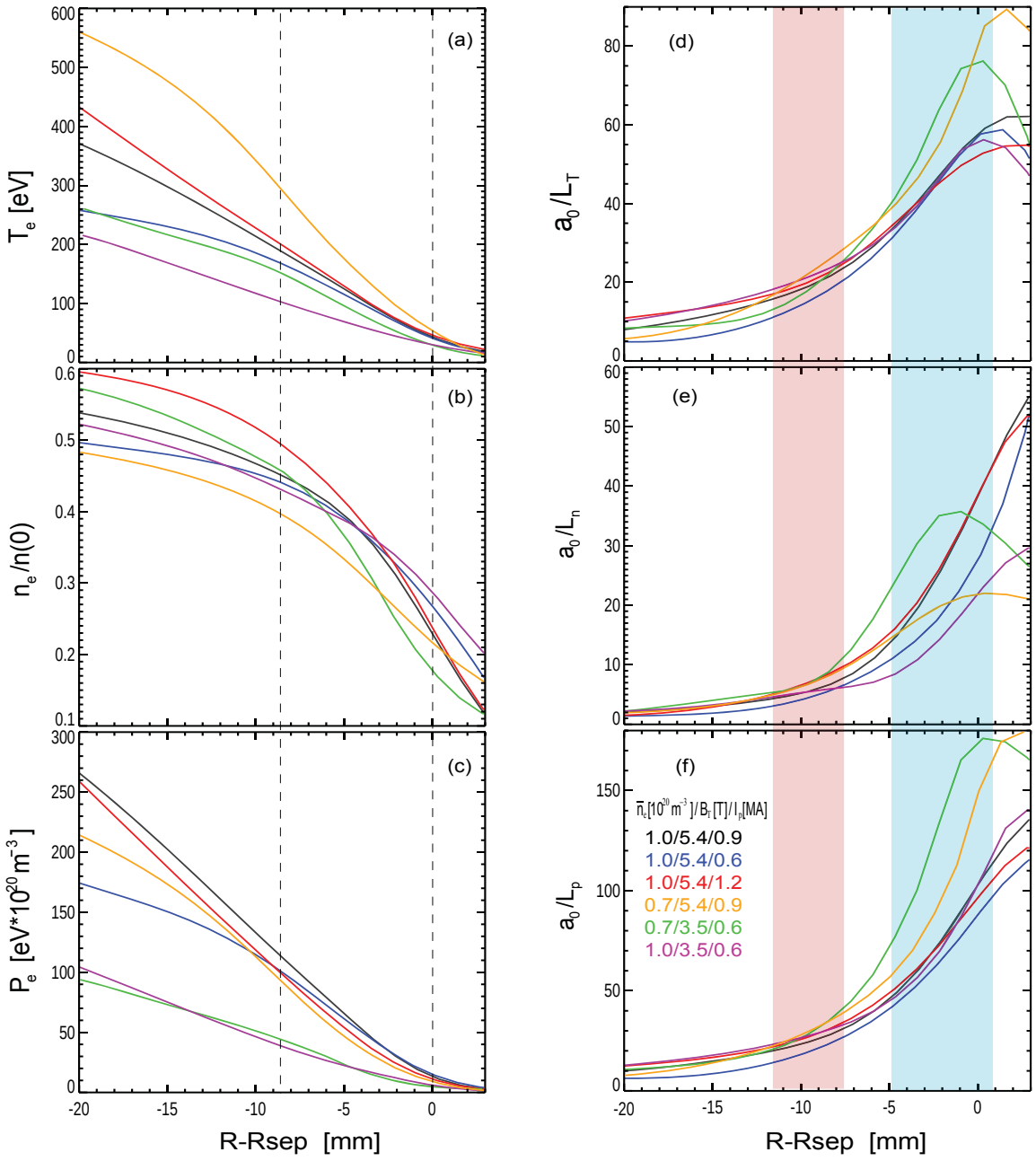

Fig.6. Composite edge profiles preceding L-H from some low density ($\bar{n}_e$<1.0x10^{20}m^{-3}) plasmas. The T_e and n_e profiles are obtained by fitting into the TS measurements from the last two laser pulses prior to L-H. Profiles of a_0/L_T and a_0/L_n are derived from the corresponding T_e and n_e profiles, respectively. Dashed lines represent the EFIT seperatrix and the approximate midplane radial location of ρ=0.95 flux surface. Shaded areas (right) are regions for spatial averaging in evaluating a_0/L_T, a_0/L_n. These profiles have been shifted in the radial direction relative to the original ones, in order to align the location of maximum d^2P_e/dr^2 (nearly the P_e pedestal foot) for each case with the EFIT separatrix.

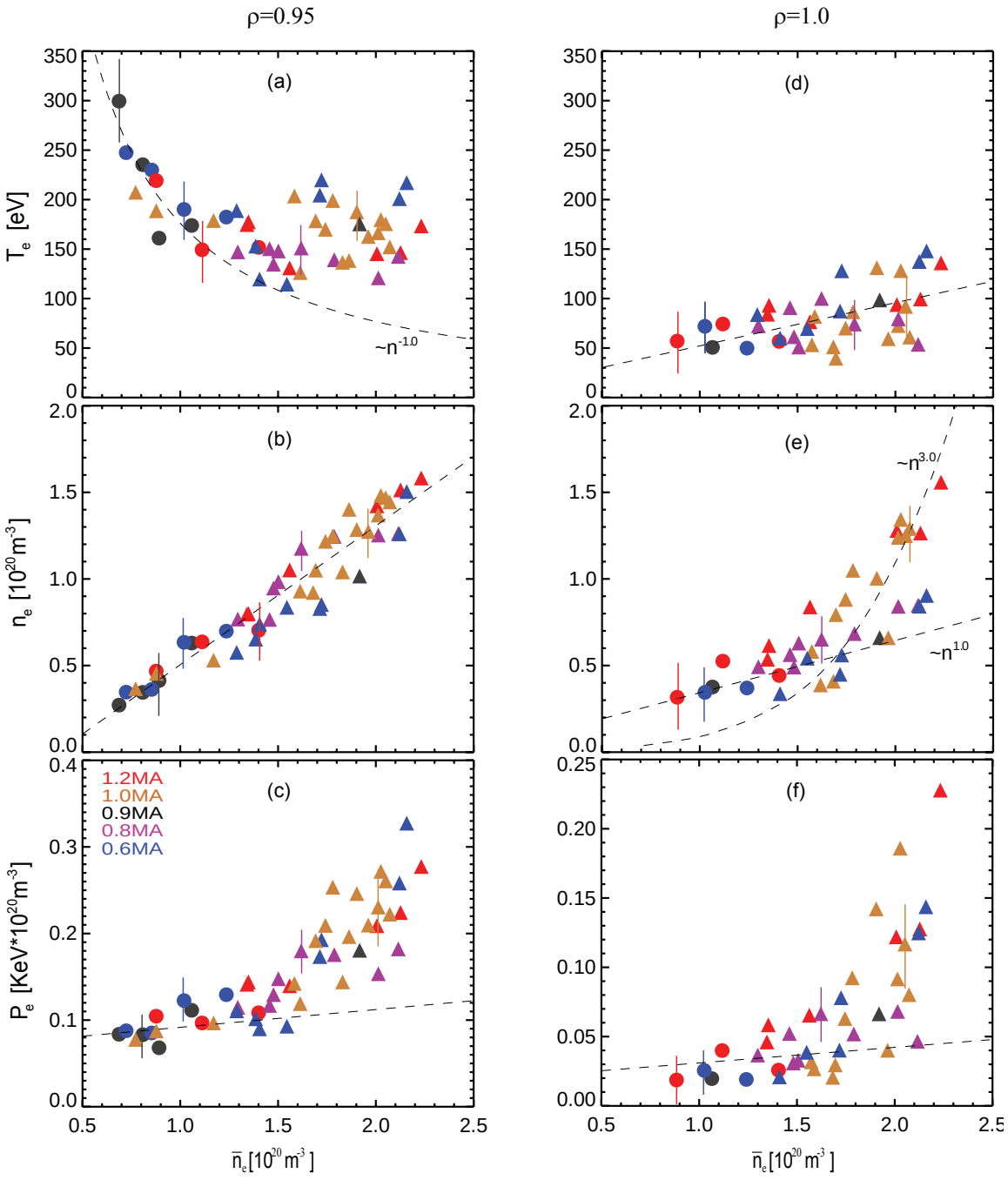

Fig.7. L-H threshold T_e, n_e, and P_e from 5.4T plasmas versus $\bar{n}_e$ at ρ=0.95 (left) and ρ=1.0 (right). Data are evaluated at the dashed lines in Fig.6 of the T_e and n_e profiles obtained by fitting into the TS data from the last two laser pulses prior to L-H. Symbol coding is identical to Fig.4. Dashed lines (except the $\sim\bar{n}_e^{\,3.0}$ one in the plot of n_e at ρ=1.0) are intended to guide the trends at low and moderate densities ($\bar{n}_e$<1.5x10^{20}m^{-3}). Only data with local n_e above ~3 x10^{19}m^{-3} are included, since this is the lower limit for reliable TS density measurements on C-Mod.

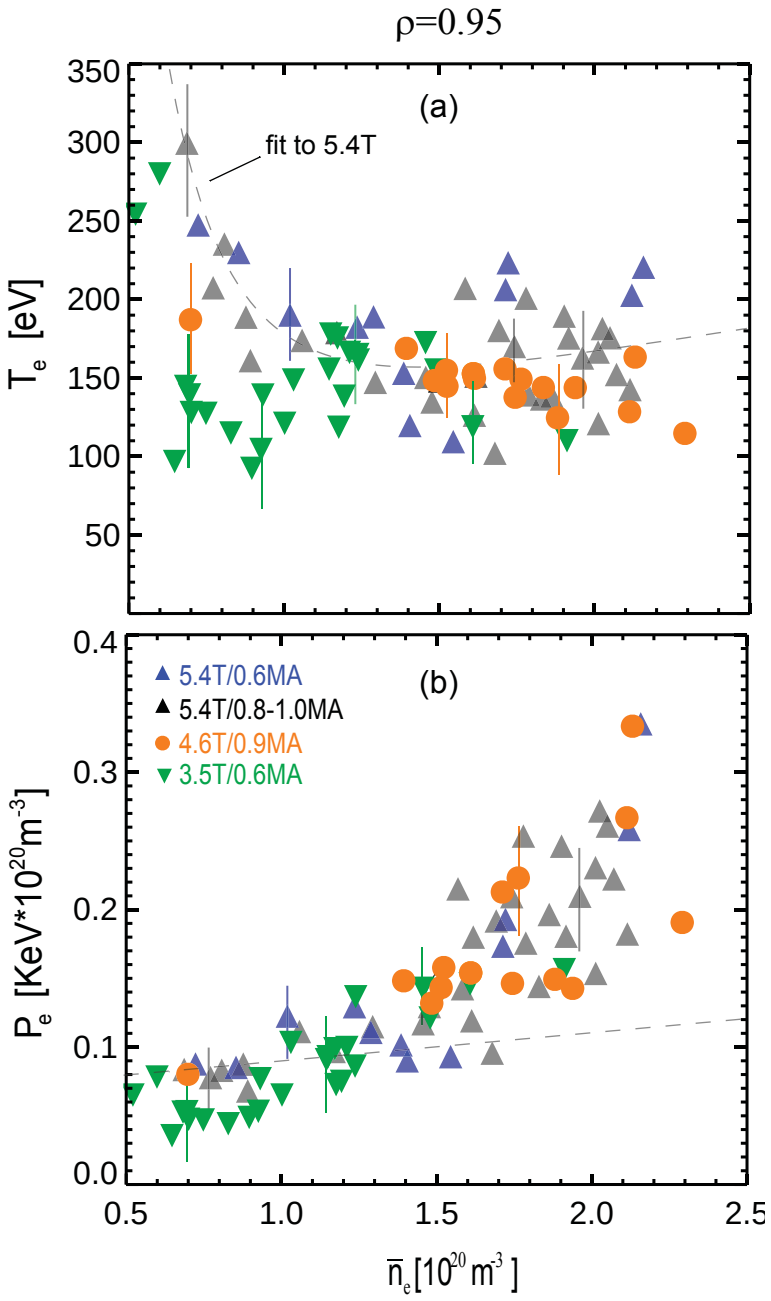

Fig.8. L-H threshold (a)T_e and (b) P_e from lower B_T (3.5T,4.6T) plasmas along with portions of 5.4T data versus $\bar{n}_e$ at ρ=0.95. The dashed line in P_e is taken from Fig.7, which is intended to guide the trend of 5.4T data in low and moderate density ($\bar{n}_e$ <1.5x10^{20}m^{-3}).

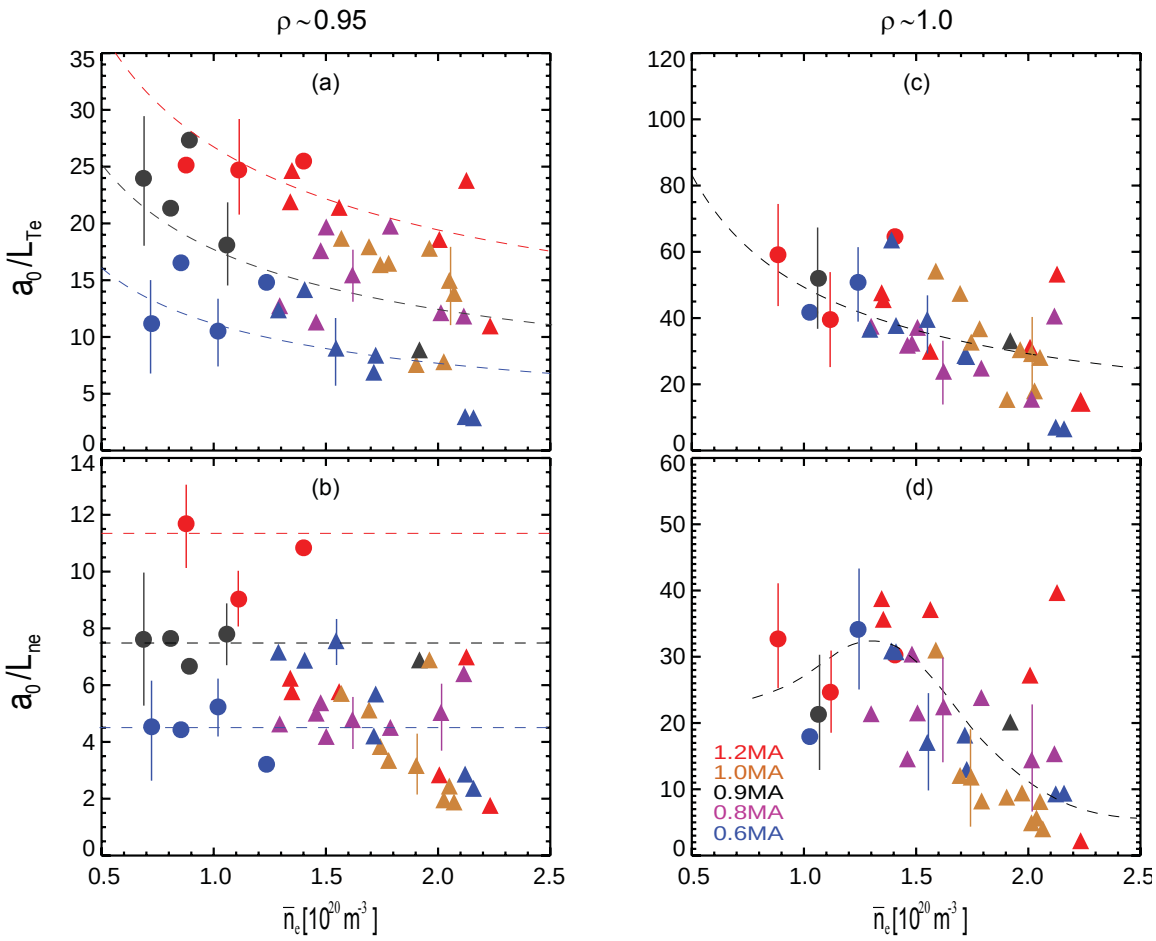

Fig.9. L-H threshold a_0/L_T, a_0/L_n from 5.4T plasmas versus $\bar{n}_e$ at ρ=0.95 (a-b) and ρ=1.0 (c-d). Data are calculated using the T_e and n_e profiles obtained by fitting into the TS data from the last two laser pulses prior to L-H, and averaged within the shaded layers in Fig.6. Symbol coding is identical to Fig.4. Dashed lines in (a) and (b) are intended to guide the trends of 5.4T data at low and moderate density ($\bar{n}_e$ <1.5x10^{20}m^{-3}). Dashed lines in (c) and (d) are intended to guide the data trend over the entire density. Some low density data have been intentionally excluded from (d) for the same reason as stated in Fig.7.

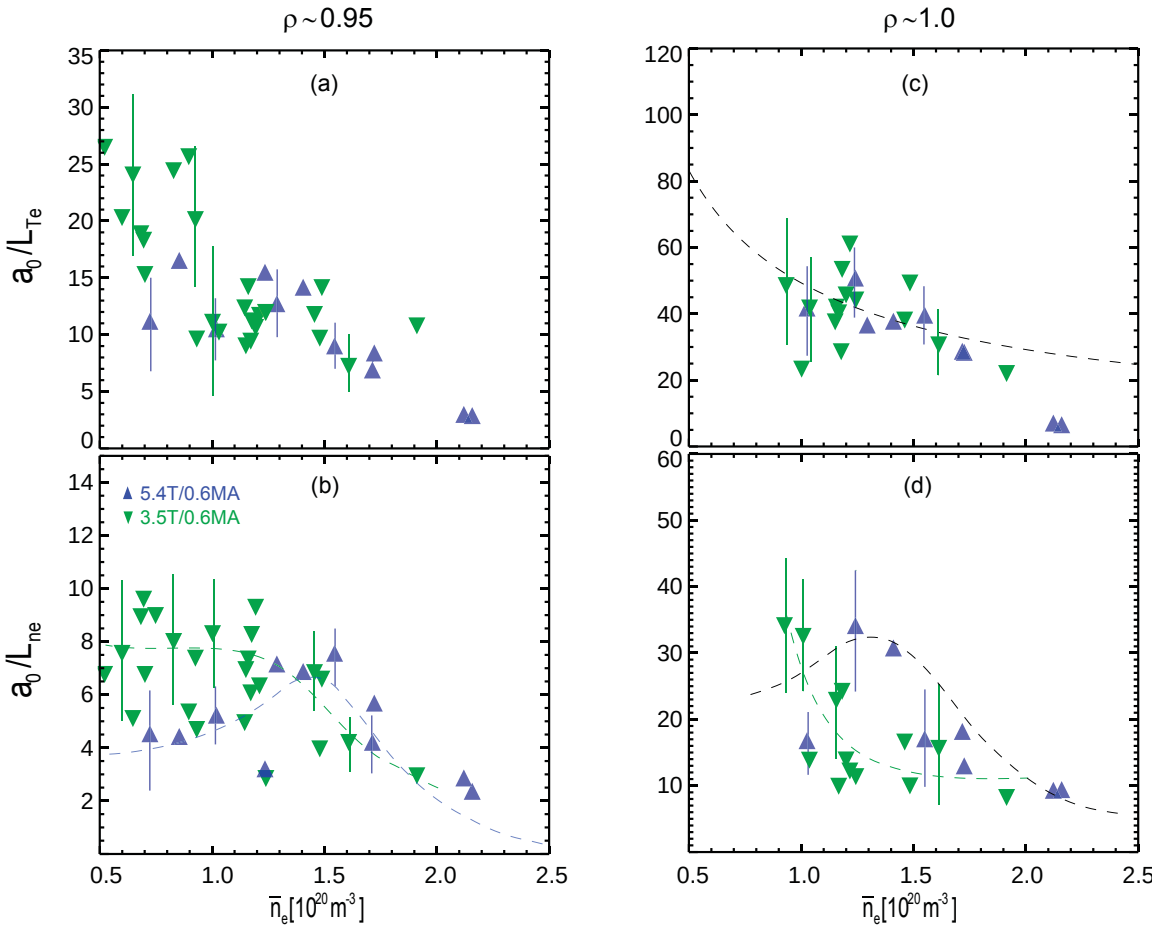

Fig.10. L-H threshold a_0/L_T, a_0/L_n from 3.5T/0.6MA plasmas along with 5.4T/0.6MA data versus $\bar{n}_e$ at ρ=0.95 (a-b) and ρ=1.0 (c-d). Data are calculated using the T_e and n_e profiles obtained by fitting into the TS data from the last two laser pulses prior to L-H, and averaged within the shaded layers in Fig.6. Dashed lines are intended to guide the data trends in 5.4T (blue), 3.5T (green), or both (black).

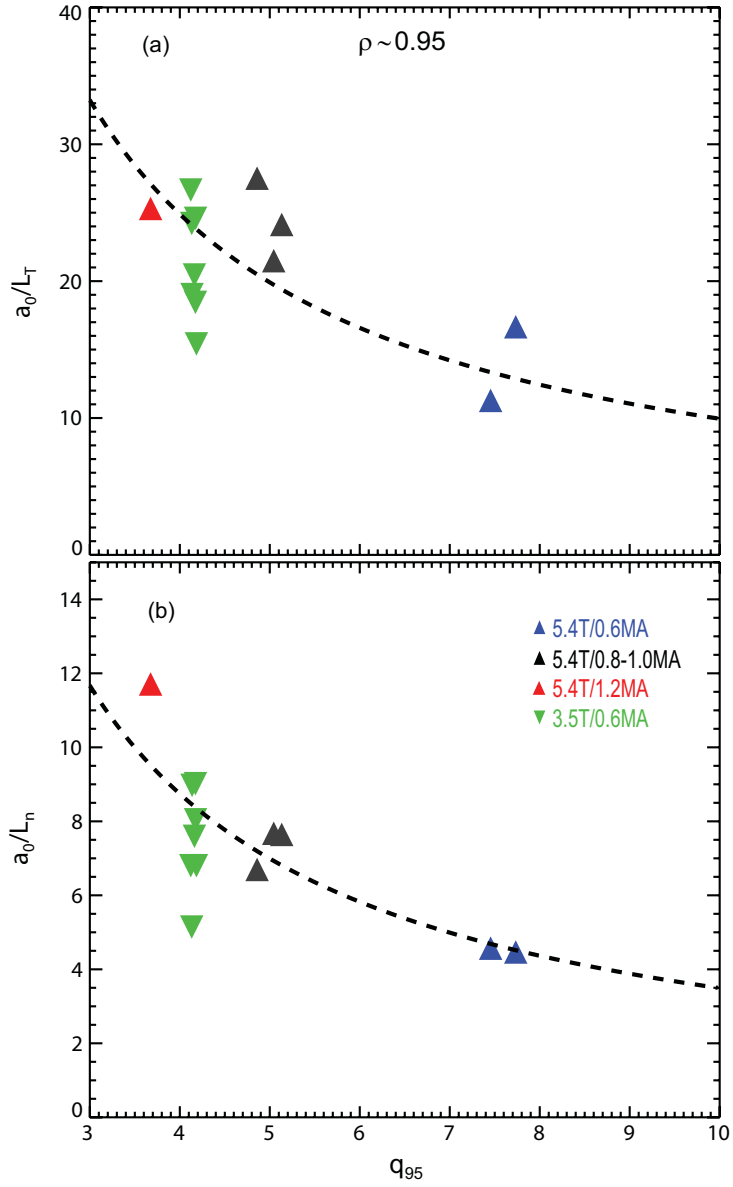

Fig.11. Data of a_0/L_{Te}, a_0/Ln_e, with $\bar{n}_e < 0.9 \times 10^{20} m^{-3}$ are displayed as a function of q_{95}. The data are found to approximately follow the $\sim 1/q_{95}$ relation, which are guided by the dashed lines on each plot.

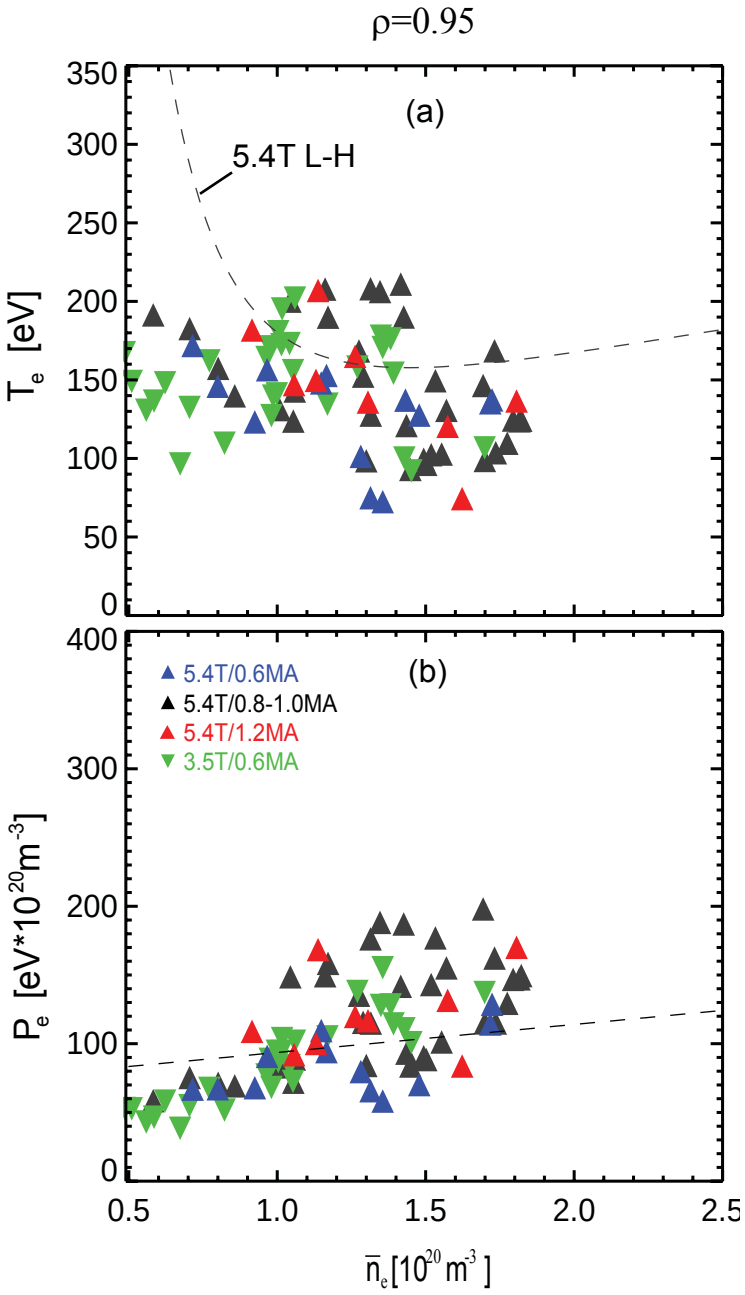

Fig.12. (a) T_e and (b) P_e in low power L-mode plasmas, versus $\bar{n}_e$ at ρ=0.95. Data are evaluated at the dashed lines in Fig.6 using T_e and n_e profiles obtained by fitting into TS data within the first 50ms of I_p flattop. Dashed lines are taken from Fig.8.

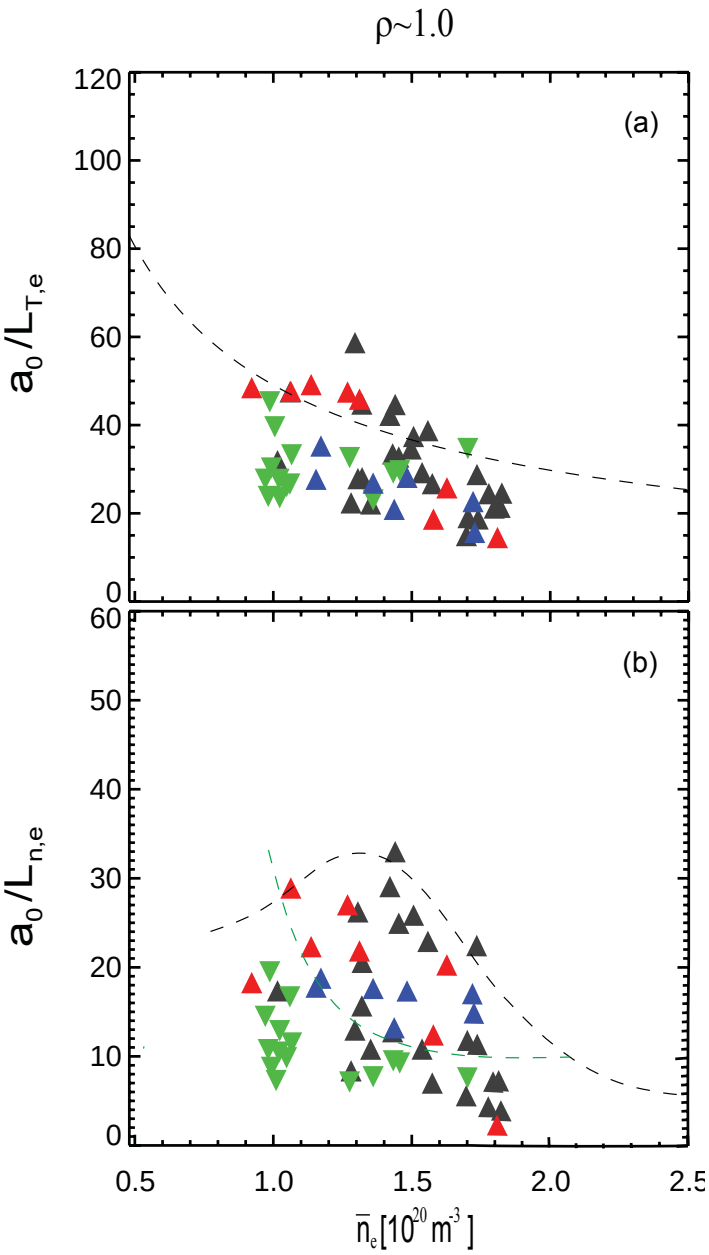

Fig.13. a_0/L_T, a_0/L_n in low power L-mode plasmas, versus $\bar{n}_e$ at ρ=1.0. Data are calculated using the T_e and n_e profiles obtained by fitting into the TS data from the first 50ms of I_p flattop, and averaged within the shaded layers in Fig.6. Dashed lines are taken from in Fig.10, which approximately guide the data trends at L-H.

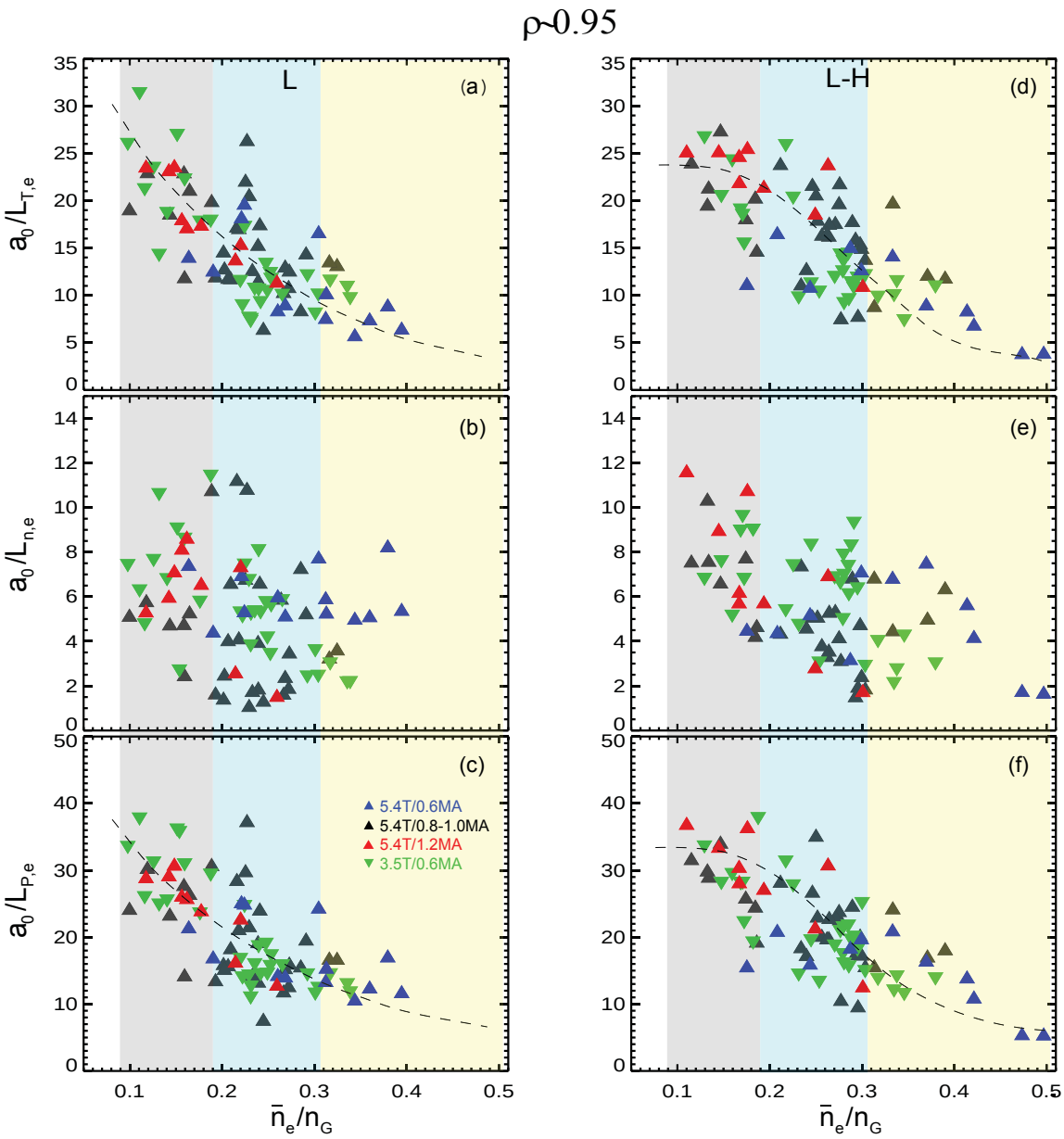

Fig.14. Illustration of a_0/L_T, a_0/L_n, a_0/L_p in low power L-mode plasmas, versus $\bar{n}_e/n_G$ at ρ=0.95, in low power L-mode (left) and at L-H (right). Dash lines are intended to guide the data trends. Shaded areas represent sheath-limited (gray), high-recycling (cyan), and detachment (yellow) regime, respectively.

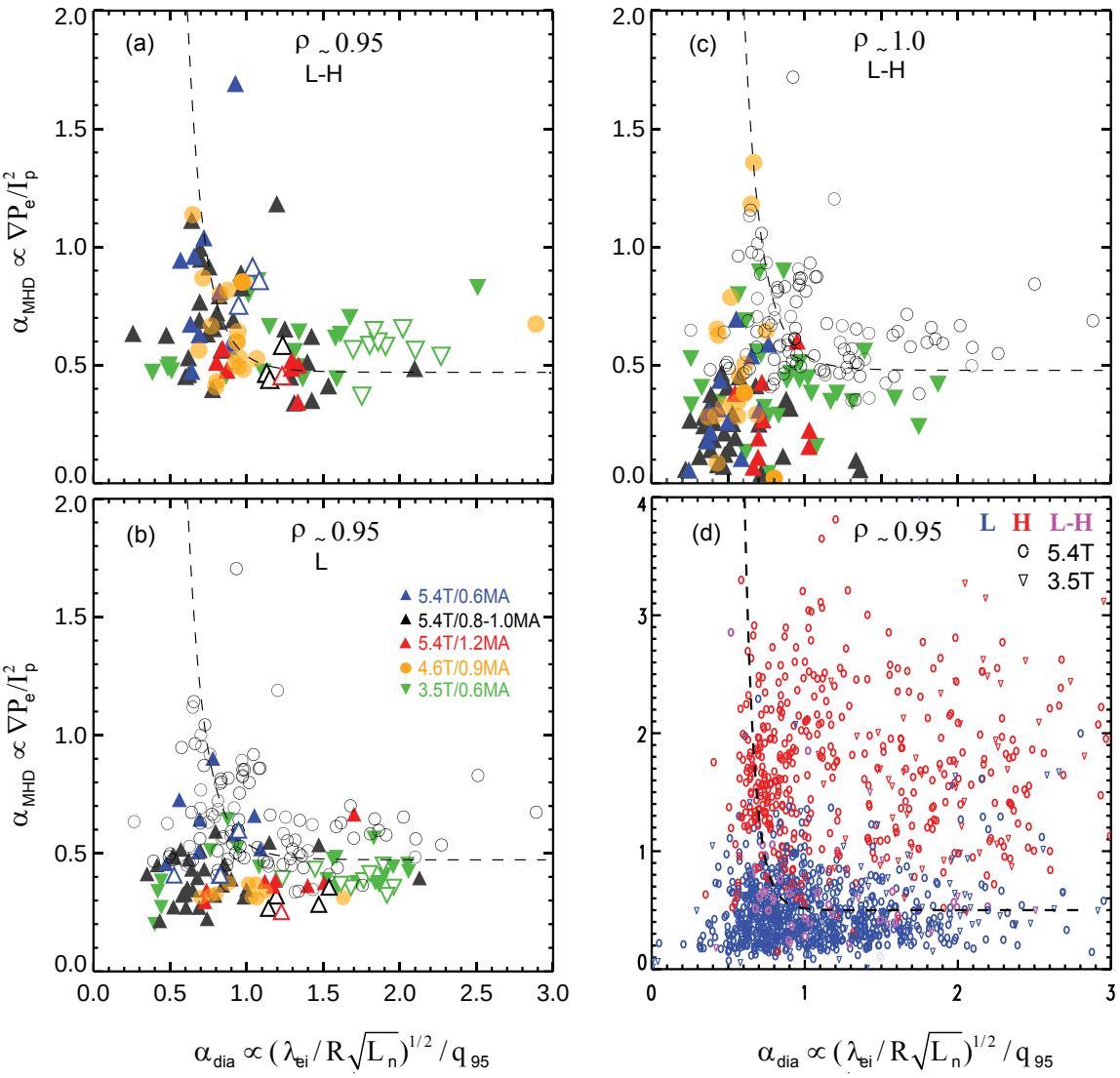

Fig.15. Plot of α_{MHD}-α_{dia} of (a) L-H at ρ=0.95 (b) Low-power L-mode at ρ=0.95 (c) L-H at ρ=0.95 (d) L-mode, L-H (last two points prior to transition), and H-mode at each TS pulse in 5.4T and 3.5T plasmas. Data from (a) are over plotted on (b) and (c) by open circles. Low density data of $\bar{n}_e < 1.0 \times 10^{20} m^{-3}$ at L-H are shown in open triangles on (a) and (b). Theory (RDZ model) predicted L-H boundary is shown by dashed line on each plot. The density coverage is $0.6 \times 10^{20} m^{-3} < \bar{n}_e < 2.1 \times 10^{20} m^{-3}$.

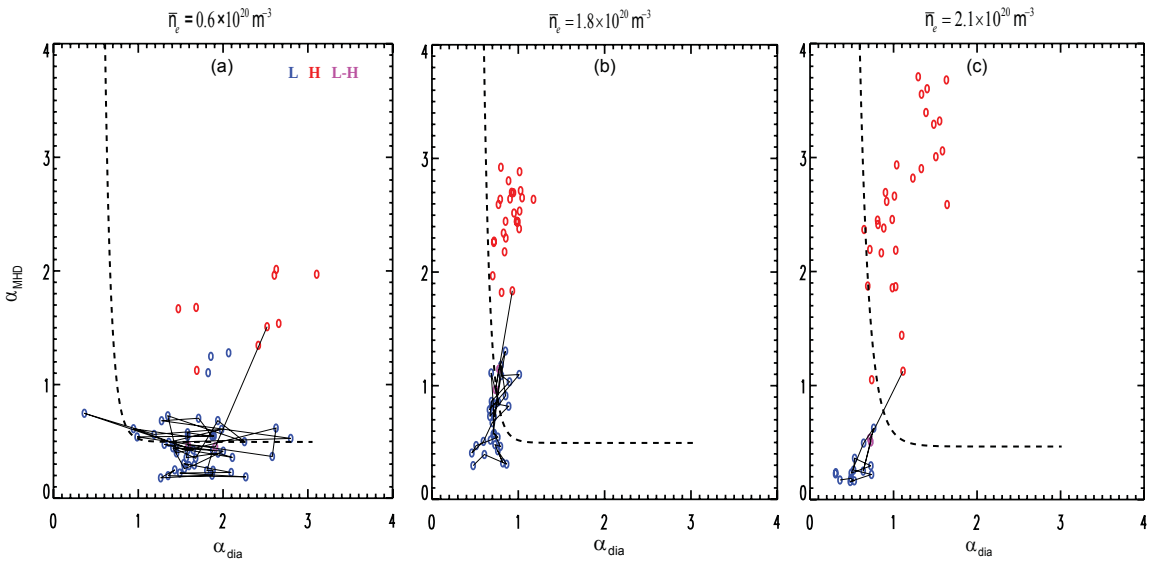

Fig.16. Comparison of time evolution of plasma states on α_{MHD}-α_{dia} diagram from L-mode to H-mode at three different plasma densities: (a) $\bar{n}_e$=0.6x10^{20}m^{-3} (b) $\bar{n}_e$=1.8 x10^{20}m^{-3} (c) $\bar{n}_e$=2.1x10^{20}m^{-3}. Each point represents a TS pulse.

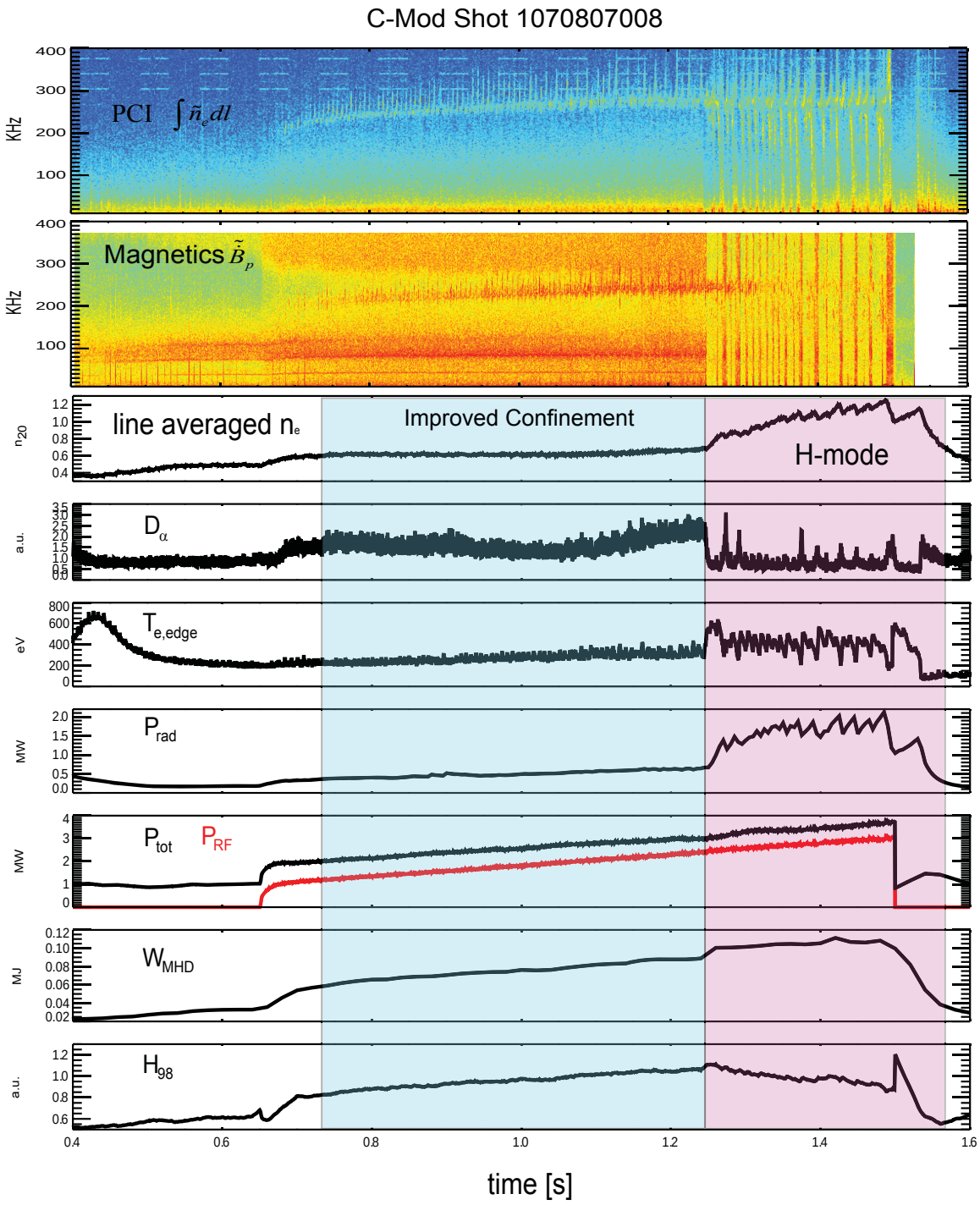

Fig.17. Time histories of global plasma parameters and plasma fluctuations in a low density discharge. Improved confinement phase lasted from 0.7s to 1.24s. H-mode was accessed at 1.24s.

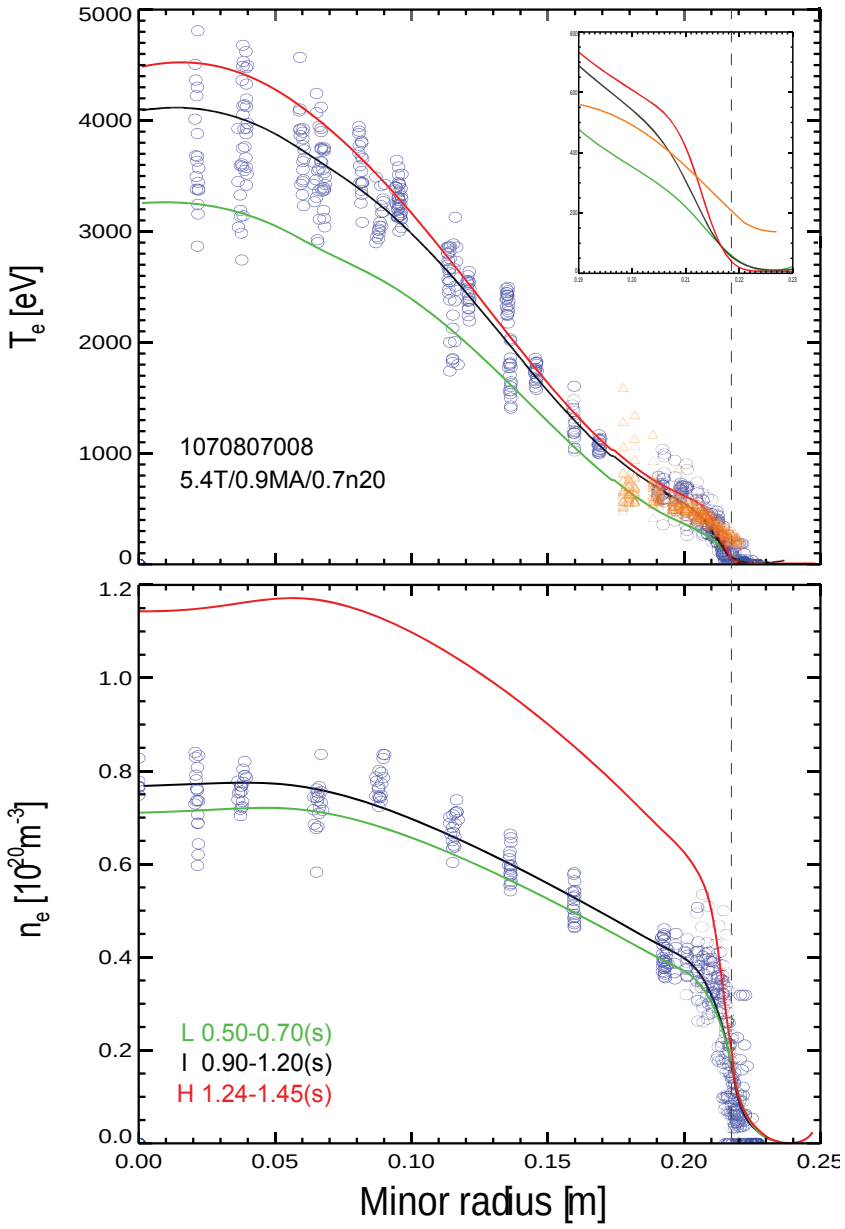

Fig.18. Time averaged T_e (top) and n_e (bottom) profiles in L-mode (green), Improved confinement (black) and H-mode (red) plasmas. TS measurements in the improved confinement phase are shown in blue open circles. The B^{5+} impurity ion temperature (T_I) measurements from charge exchange recombination spectroscopy in the same time period are represented by yellow triangles in the top panel.